Astron. Astrophys. 85, 36–54 (1980)

ASTRONOMY AND ASTROPHYSICS

# Multifrequency Observations of Very Large Radio Galaxies

## II. 3C236

R. G. Strom[1] and A. G. Willis[2]*

[1] Netherlands Foundation for Radio Astronomy, Radiosterrenwacht Dwingeloo, Postbus 2, NL-7990 AA Dwingeloo, The Netherlands

[2] Sterrewacht Leiden, Postbus 9513, NL-2300 RA Leiden, The Netherlands

Received April 17, 1979

**Summary.** The large double radio source 3C236 has been observed with the Westerbork telescope at wavelengths of 6, 21, and 49 cm. In the outer components, which together span a distance of nearly 4 Mpc, we have mapped the total intensity and linearly polarized brightness distributions. These have enabled us to study spatial variations in the spectral index, rate of depolarization, rotation measure and magnetic field structure. We find them all to possess quite simple distributions. There is marginal evidence that the spectral index steepens away from the components' leading edges: We conclude that some form of particle (re)acceleration must occur throughout the radio lobes, including those featureless regions where there is no apparent sign of activity. 3C236 possesses a high degree of linear polarization with only slight depolarization between 21 cm and 49 cm, while the rotation measure within each component is nearly constant. The magnetic field is quite uniform, generally runs parallel to contours in the total intensity distribution, and has a high degree of order.

We find morphological evidence for the presence of several generations of subcomponents and suggest that they are a principal mechanism by which the outer lobes have been energized. From estimates of their speed we conclude that 3C236 may be $10^{11}$ yr old. Furthermore, we show that the component shape may to some extent be determined by events near the optical nucleus. The associated galaxy is probably very massive, and the fact that it appears to be isolated as well as in a region of very low density raises questions about the formation of ellipticals. Finally, we note that the presence of extensive magnetic fields in sources like 3C236 implies a low upper limit to the mass of the photon.

**Key words:** radio galaxies – magnetic fields – energy transport – radio source morphology – intergalactic material

## 1. Introduction

In this, the second in a series of papers presenting multifrequency radio observations of very large (at least 1 Mpc in overall extent) radio galaxies, we discuss 3C236. Paper I (Willis and Strom, 1978) presented observations of the 1.7 Mpc galaxy 3C326. The subject of the present paper was shown by Willis et al. (1974) to be an immense radio galaxy: its 40′ angular extent corresponds to a linear size (for $H_0 = 75\,\mathrm{km\,s^{-1}\,Mpc^{-1}}$) of nearly 4 Mpc.

*Send offprint requests to:* R. G. Strom

* Present address: Radiosterrenwacht Westerbork, Schattenberg 4, NL-9433 TA Zwiggelte, The Netherlands

Between the extended outer components of 3C236 lies a compact radio source. All position, flux density, polarization and other similar measurements made before 1974 refer to this component, and strictly speaking, it alone ought to be called 3C236. Interesting in its own right, the central source has been shown to have structure on a much smaller scale extending along the same position angle as that of the outer components (Wilkinson, 1972; Fomalount [sic] and Miley, 1975).

The present observations were made to study the structure of the two outer components at 6 cm (4995 MHz), 21 cm (1415 MHz), and 49 cm (610 MHz) using the Westerbork Synthesis Radio Telescope (WSRT). We present the results in a format similar to that used in Paper I. For convenience, we will refer to the northwest component as 1002+35 and the southeast one as 1004+34.

## 2. Observations

Table 1 lists the observational material we have obtained. The resulting map parameters are summarized in Table 2. For general details of the data reduction procedure we refer the reader to Paper I and references therein. Two special circumstances make the data reduction more complicated than it was for 3C326 (Paper I).

First, the surface brightness contrast between the nuclear source and outer lobes of 3C236 in our 49 cm and 21 cm observations is as much as $10^3$ in places. These measurements are thus frequently dynamic range limited (though in the polarization

**Table 1.** Observing log for 3C236

| Wavelength (cm) | Field | Field center (1950.0) RA | Dec | Time (h) | Spacings[a] (m) | Date |
|---|---|---|---|---|---|---|
| 49.2 | 3C 236 | $10^h04^m00^s$ | 35°00'00" | 2 x 12 | 36, 36, 1440 | 1974.2, 1974.5 |
| 21.2 | 3C 236 | 10 03 05.4 | 35 08 48 | 4 x 12 | 36, 18, 1458 | 1974.6, 1974.8 |
| 6.0 | 3C 236 (east) | 10 04 38 | 34 56 15 | 2 x 12 | 36, 36, 1440 | 1974.9, 1975.0 |
| | 3C 236 (west) | 10 02 15 | 35 15 50 | 2 x 12 | 36, 36, 1440 | 1975.9, 1976.0 |
| | 3C 236 (nucleus) | 10 03 05.05 | 35 08 49 | 2.4 | 72, 72, 1440 | 1976.5 |

[a] Listed in order of shortest baseline, increment, longest spacing

**Table 2.** Westerbork map parameters for 3C236

| Wavelength (cm) | 49.2 | 21.2 | 6.0 |
|---|---|---|---|
| Primary beam half power width (arc min) | 82 | 37 | 11 |
| Normal synthesized beam half power width (arc s, RA x Dec) | 55 x 96 | 23 x 40 | 7 x 12 |
| Distance between grating responses (arc min, RA x Dec) | 46 x 80 | 40 x 70 | 5.6 x 9.8 |
| Total intensity r.m.s. noise (mJy/synthesized beam) | 2.2 | 0.5 | 0.7 |
| Polarization r.m.s. noise (mJy/synthesized beam) | 1.0 | 0.2 | 0.7 |

maps and where the total intensity emission is weakest noise is also significant). The gain and phase stability during the 49 cm observations were typically 1% and 1°, respectively, so significant distortion occurs only within a few beamwidths of the central component.

At 21 cm the data quality is not quite as good, but because of higher resolution the surface brightness observed in the outer lobes is much less than that of the (unresolved) central component. As a result, a map made from the raw data is significantly contaminated by instrumental responses from this source, mainly caused by short term phase variations. A research project being carried out by Hamaker (1978) has identified a major source of the phase fluctuations as irregularities in the troposphere. Similar defects have been discussed by Hinder and Ryle (1971). By an adaptive filtering technique, Hamaker (in preparation) has used the strong central component as a phase reference and removed the tropospherically produced short term phase jitter from the data. This resulted in a decrease of most of the spurious sidelobes to a level under 0.1%.

At 6 cm the size of the primary beam effectively limits the field of view so that each outer component could be observed free of contamination by the central source.

The second effect it was necessary to correct for is instrumental polarization at 21 cm. A parabolic reflector illuminated by an electric dipole suffers from the well-known "barrel" distortion (Christiansen and Högbom, 1969). While modern feed design attempts to minimize the resulting off-axis spurious polarization by matching the E- and H-plane illumination, small differences can produce a significant effect far from the beam center. This is important for a source 40′ in extent, as 3C236 is, since the primary beam half power width is only 37′ (Table 2). Using the known 21 cm polarization properties of the WSRT (Weiler et al., 1973) and the fact that the outer components of 3C236 cover a narrow range of position angles relative to the location of the field center, we have removed average instrumental polarizations of 5% and 1.5% oriented in position angle 122°.5 from 1004+34 and 1002+35, respectively.

## 3. Results

For convenience during the discussion which follows, five peaks in and near the outer lobes of 3C236 have been labelled $A-E$. Most of them are probably background sources unrelated to 3C236. They are indicated in those total intensity contour plots where they appear as separate peaks.

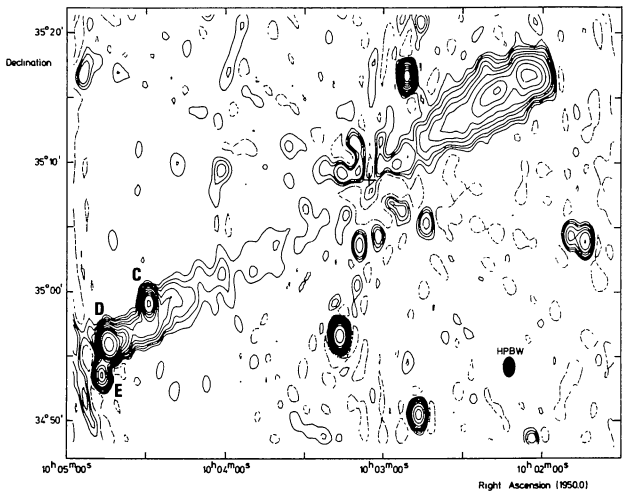


**Fig. 1.** A contour plot showing the total intensity distribution of 3C236 at a wavelength of 49 cm. The compact 5 Jy central source has been subtracted off and its position is indicated by a cross. (Positive and negative features within 3′ to 4′ of the cross are instrumental residuals of this source.) Contour values are: −5 (dashed), 5, 10, 15, 25, 35, 50, 75, 100, 125, 150, 200, 300, and 400 mJy/synthesized beam. Letters indicate peaks discussed in the text. In this and the following figures, a shaded ellipse near one corner shows the half power synthesized beam width (HPBW)

*a) 49 cm Wavelength*

The original 49 cm map presented by Willis et al. (1974) was not corrected for primary beam attenuation. Figure 1 shows the final version, so corrected, together with the linearly polarized intensity (Figs. 2a and 3a) and corresponding degree of polarization (Figs. 2b and 3b).

The smooth emission from 1002+35 shows that even with 1′ resolution the component exhibits no significant regions of unresolved structure. It is noteworthy that the degree of polarization is lowest along the ridge of maximum total intensity, rising to more than 30% near the northern and southern edges of the component. Moreover, minima of less than 5% are found close to the two peaks in the total intensity emission (in both cases displaced just to the northwest). The high degree of polarization (exceeding 50%) near $RA = 10^h02^m.6$, Dec = 35°13′.5 is caused by a peak in the polarized intensity (Fig. 2a) at this position.

The structure of 1004+34 is a striking contrast to that of the preceding lobe. In and near the eastern half of the component three peaks have been marked. The on-axis one (*D*), which is unresolved on its "leading" edge but blends smoothly into the lower brightness plateau to the northwest, is clearly the outer hot spot one often finds in radio components. Willis et al. (1974) argued that the other two (*C* and *E*) are likely to be background sources. Later we will discuss new evidence relating to this point.

The degree of polarization in 1004+34 rises to 30% in places (Fig. 3b) similar to the values found in 1002+35. No polarized flux emanates from peak *E*. Near peak *C*, the degree of polarization drops from about 15%, to 5% on the peak itself, strongly suggesting that *C* contributes nothing to the polarized emission. As in 1002+35, the higher brightness regions of 1004+34 (especially the hot spot *D*) have a lower degree of polarization. However, there is no apparent increase north and south of the main emission ridge as noted in 1002+35.

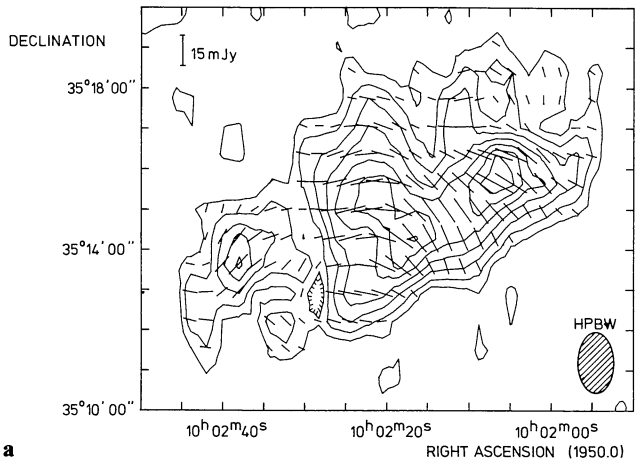


a

**Fig. 2a and b.** The linear polarization distribution in 1002+35 at 49 cm. **a** The linearly polarized intensity, $(Q^2+U^2)^{1/2}$, shown as contours and the position angle of the electric vector, $\frac{1}{2}\arctan(U/Q)$, shown as "vectors". Contour values are: 3, 5, 7.5, 10, 12.5, 15, and 17.5 mJy/synthesized beam. **b** Contours showing the degree of polarization (in %) superimposed on a radio photograph of the total intensity distribution. Minima and maxima are indicated by "<" and ">", respectively

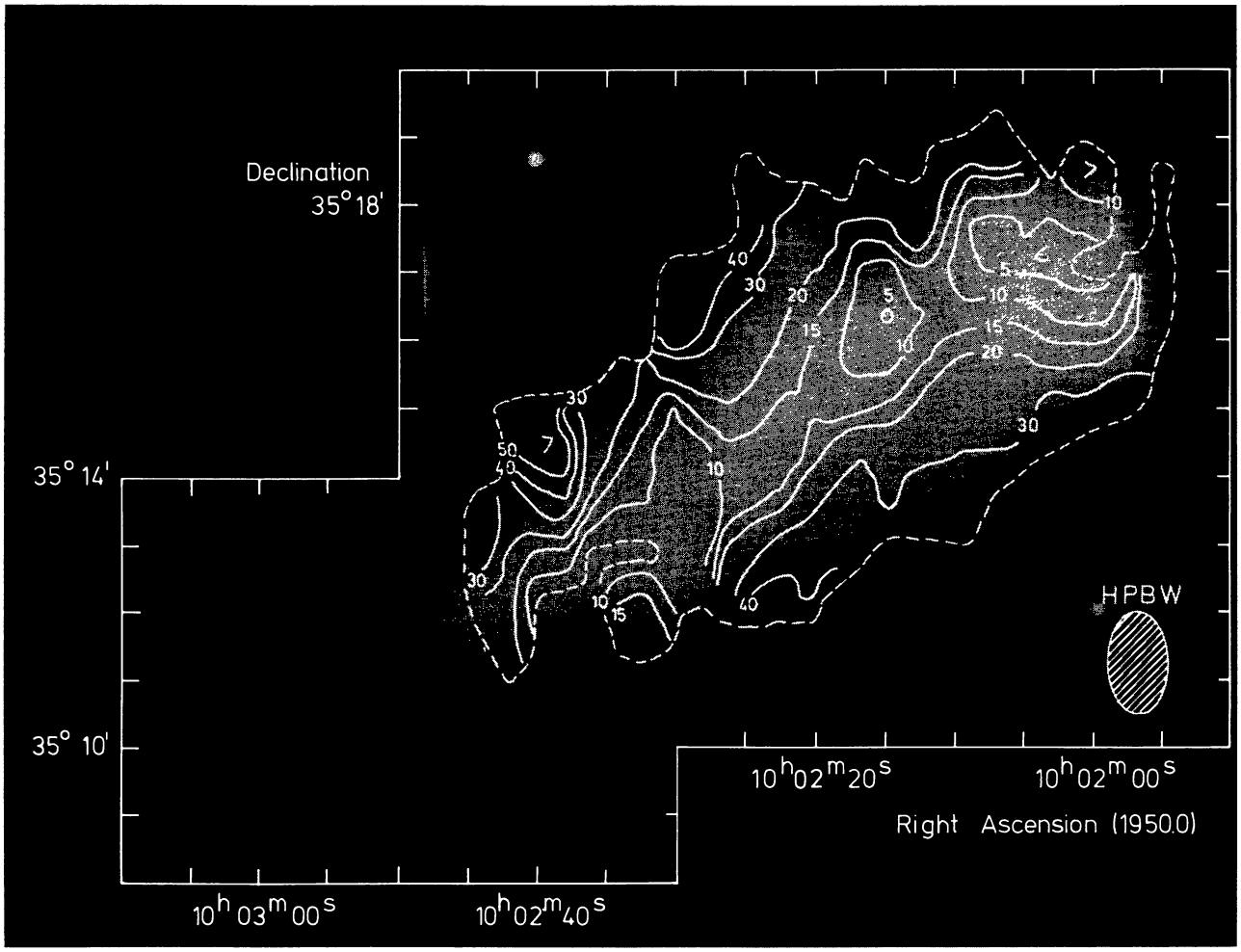


b

*b) 21 cm Wavelength*

The conclusion we drew from the 49 cm map, that there are no significant regions of unresolved emission in 1002+35 is confirmed by the 21 cm map (Fig. 4a) in almost every respect. The notable exception is the ridge of emission which runs parallel to and slightly north of the component's central axis, its intensity rising to a peak near $RA = 10^h02^m15^s$, Dec. $= 35°16'$. This feature, with its unresolved leading edge and low brightness tail, has the hallmarks of a typical radio source component. What is unusual is that it is surrounded by, and presumably immersed in, the smooth trailing emission of a much larger component which has its own brightened (though fully resolved) leading end.

Apart from the compact interior component, none of the emission in 1002+35 remains unresolved by the 21 cm beam.

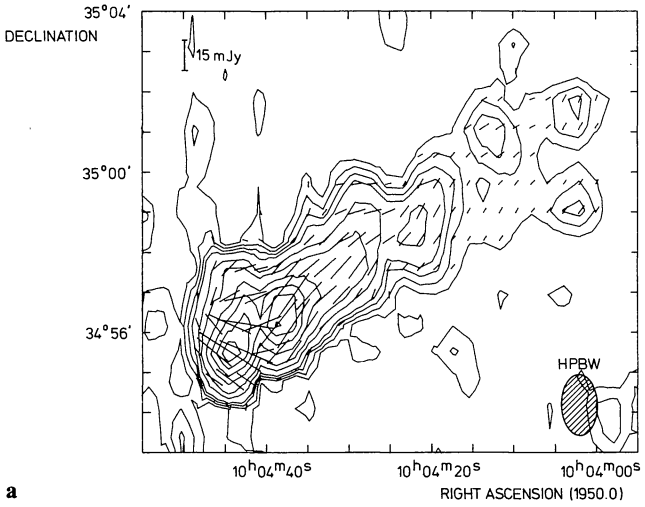


a

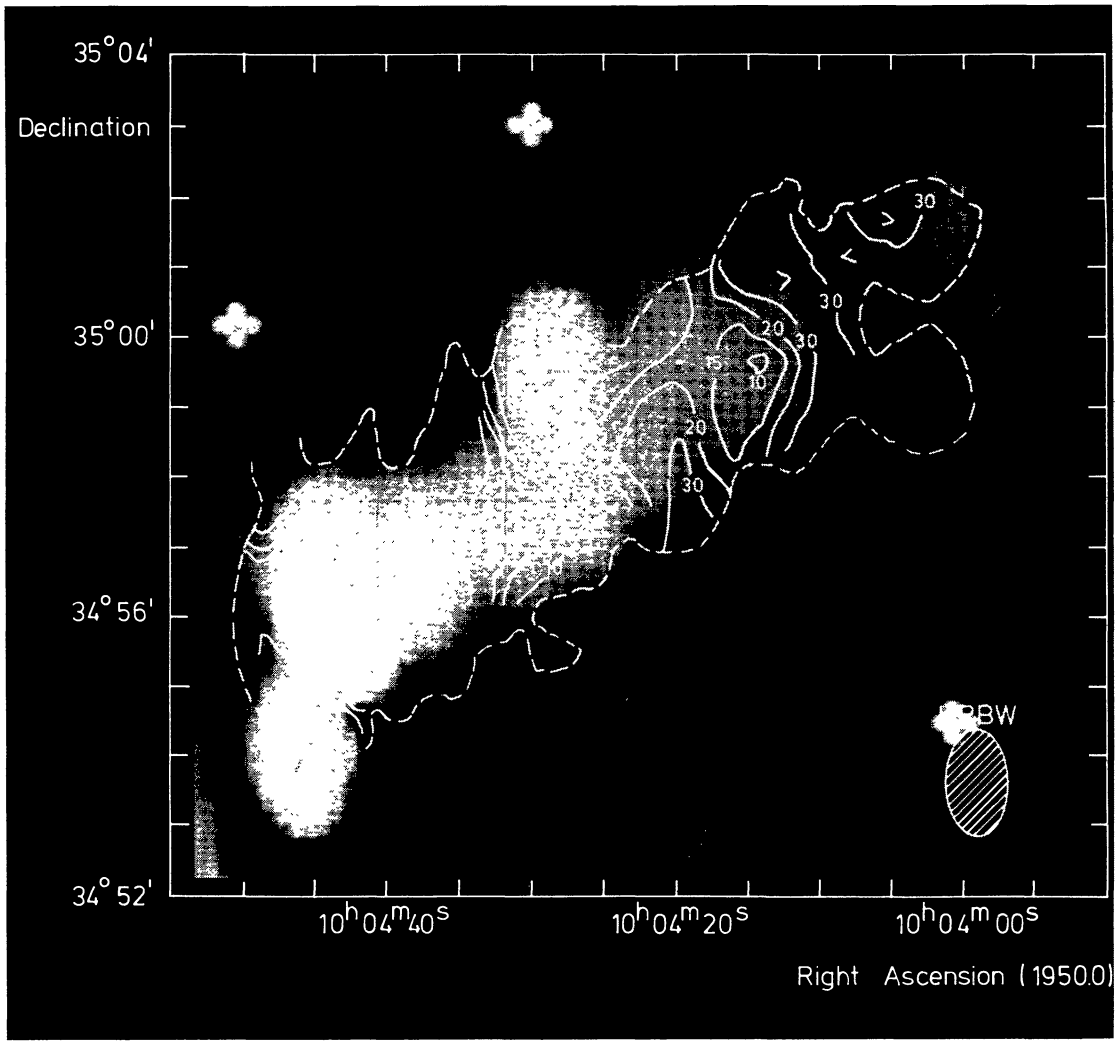


b

**Fig. 3a and b.** The 49 cm linear polarization distribution in 1004+34. **a** Contours of the linearly polarized intensity and "vectors" showing the position angle of the electric vector. Contour values are: 2, 3, 4, 5, 7.5, 10, 15, 20, 25, and 30 mJy/synthesized beam. **b** Contours showing the degree of polarization (in %) superimposed on a radio photograph of the total intensity distribution

(Peak *A* is probably unrelated to 3C236, the emission which appears to link it to 1002+35 being caused by a weak residual grating response: Note the adjacent negative ridge to the east. Although source *A* has no optical counterpart to the limit of a deep Kitt Peak 4 m plate kindly made available by E. Burbidge, we have no reason to suppose it is anything but a background source.) Apart from several spur-like protrusions, the higher brightness region on the western end is largely featureless and slightly reminiscent of the eastern component in 3C326 (Paper I). To the east the emission from 1002+35 dies gradually away, but because of the strength of the central component it is difficult to know whether it extends all the way to the center.

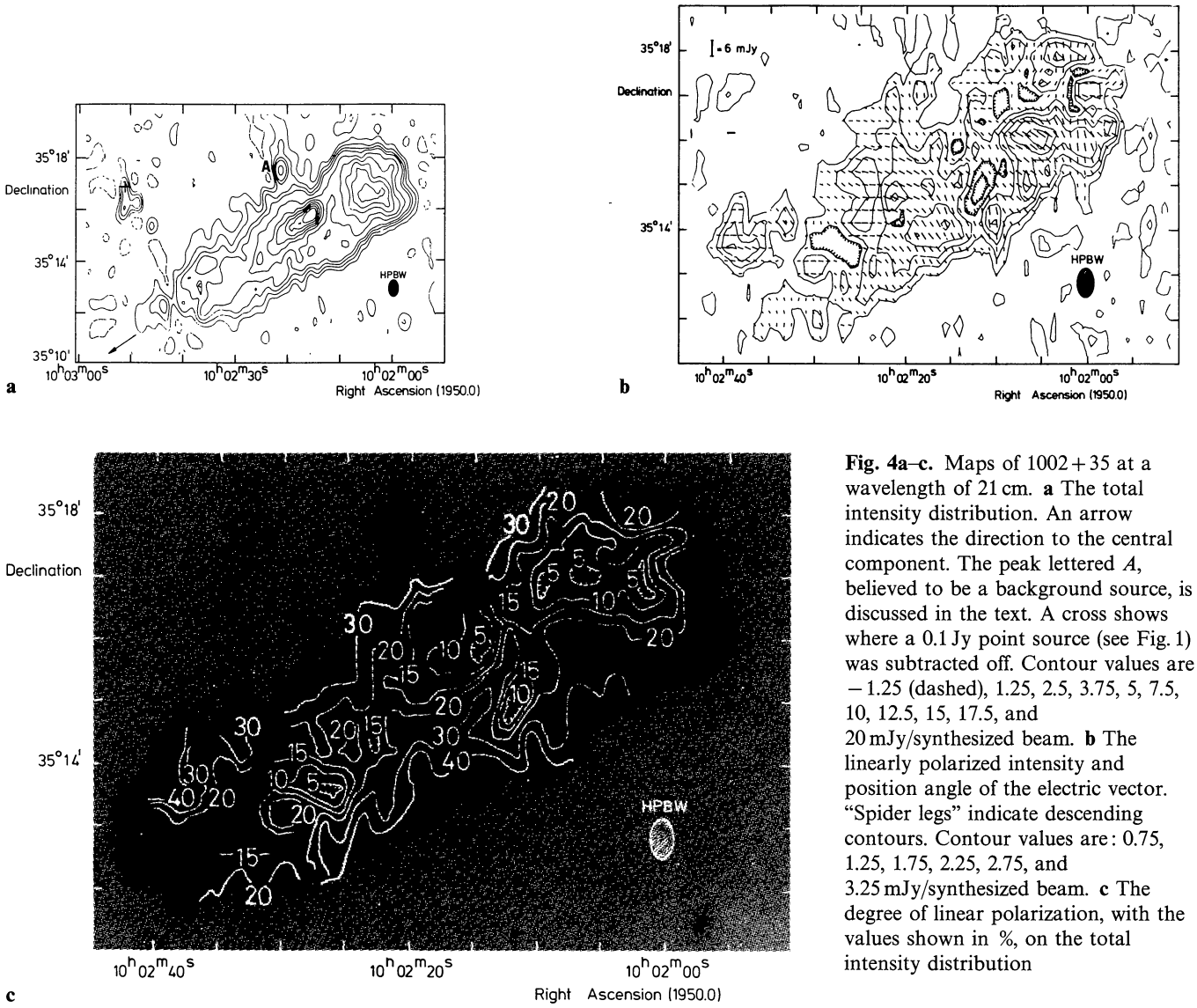


**Fig. 4a–c.** Maps of 1002+35 at a wavelength of 21 cm. **a** The total intensity distribution. An arrow indicates the direction to the central component. The peak lettered *A*, believed to be a background source, is discussed in the text. A cross shows where a 0.1 Jy point source (see Fig. 1) was subtracted off. Contour values are: −1.25 (dashed), 1.25, 2.5, 3.75, 5, 7.5, 10, 12.5, 15, 17.5, and 20 mJy/synthesized beam. **b** The linearly polarized intensity and position angle of the electric vector. "Spider legs" indicate descending contours. Contour values are: 0.75, 1.25, 1.75, 2.25, 2.75, and 3.25 mJy/synthesized beam. **c** The degree of linear polarization, with the values shown in %, on the total intensity distribution

The distribution of polarized emission (Fig. 4b) reflects few of the features found in the total intensity map. In particular, there is no hint of the interior ridge, though its outer unresolved edge coincides with a minimum in the polarized intensity. The strongest polarization emanates from the countermost region. Minima in the polarized intensity often occur where the position angle changes rapidly, suggesting they are the result of vector cancellation caused by beam smearing of adjacent, orthogonally polarized regions. Their influence is also seen in low points in the degree of polarization (Fig. 4c). The strongly polarized peak near $10^h02^m.6$, 35°13′.5 noted in the 49 cm map is also present at 21 cm. Except for this feature, the southern part of 1002+35 is generally more strongly polarized than the northern half.

The greater resolution obtained at 21 cm is used to full advantage in the map of 1004+34 (Fig. 5a). In the region of the outer hot spot (peak *D*) especially, there is more detail than at 49 cm. Although the leading edge remains unresolved, it is clear that the emission peak is near the southern end of the ridge. As in typical source components, emission behind the peak steadily dies away, though there are traces of it more than 10′ from the outer edge.

In addition to peaks *C* and *E*, a new one (*B*) appears on the northern edge of the component at 21 cm. We have searched for optical counterparts to these three candidate background sources: *B* coincides with a $\sim 20^m$ blue stellar object clearly visible on the Palomar Sky Survey O print; for *C* we find a faint $\sim 22^m$ to $23^m$ object visible only on the deep 4m Kitt Peak IIIa-J plate; *E* has no optical counterpart. Neither object associated with *B* and *C* could be seen on correspondingly deep red prints. Source *E*, although unidentified, is clearly separate from 1004+34, resolved into a double, and we have no reason to believe it is other than a background source. Properties of the four lettered background sources are summarized in Table 3.

The strongest polarization in 1004+34 (Fig. 5b) coincides with the outer peak (*D*) of the total intensity map. The highest degree of polarization (Fig. 5c) is, however, found in the weaker emission behind the leading edge. The abrupt drop in polarization near $10^h04^m45^s$, 34°56′.4 occurs where the position angle changes rapidly, and is thus similar to minima observed in 1002+35. It is noteworthy that no significant polarized flux is detected along the southern edge of the component between $10^h04^m27^s$ and $10^h04^m37^s$, implying a degree of polarization which is everywhere

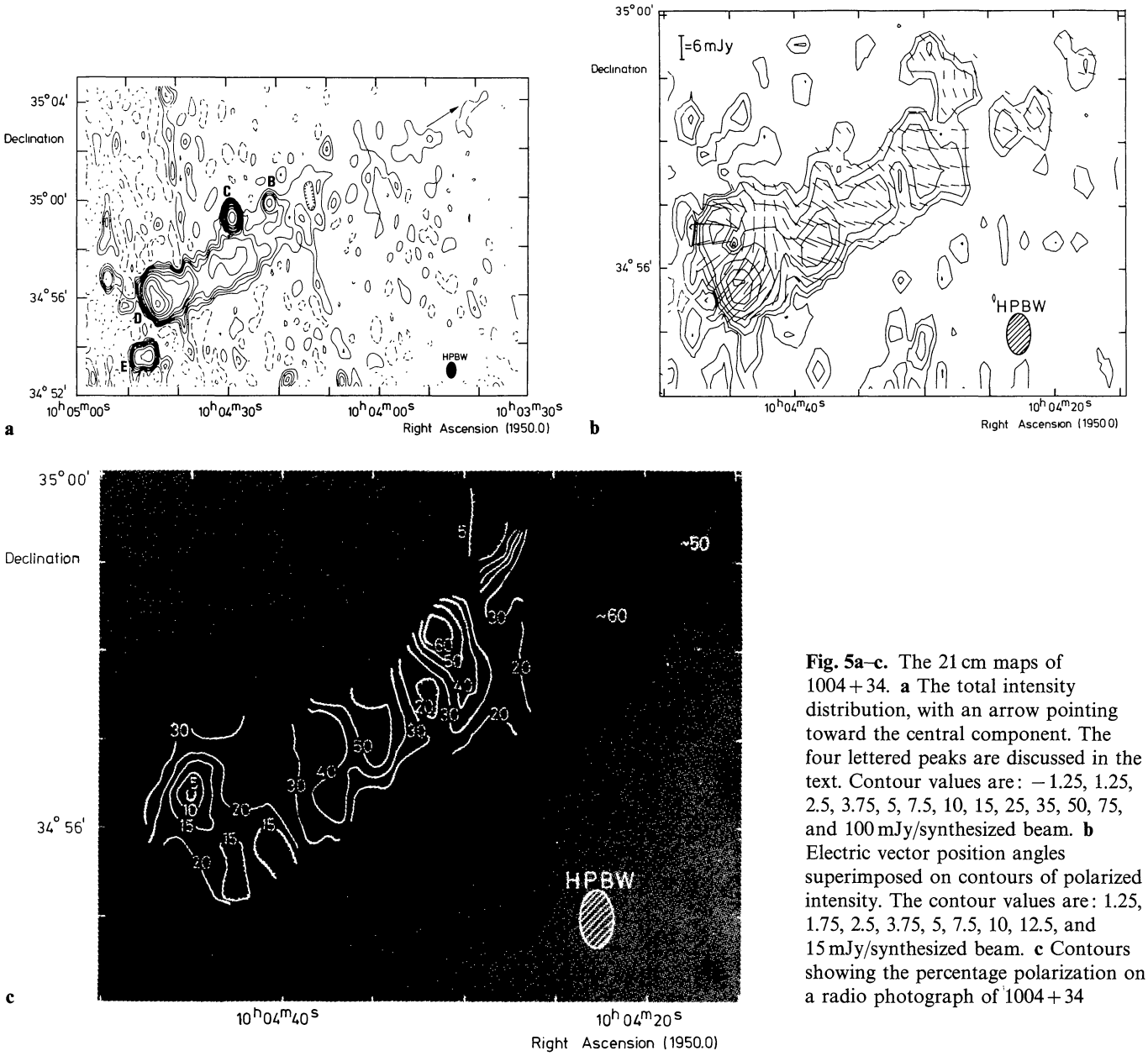


**Fig. 5a–c.** The 21 cm maps of 1004+34. **a** The total intensity distribution, with an arrow pointing toward the central component. The four lettered peaks are discussed in the text. Contour values are: −1.25, 1.25, 2.5, 3.75, 5, 7.5, 10, 15, 25, 35, 50, 75, and 100 mJy/synthesized beam. **b** Electric vector position angles superimposed on contours of polarized intensity. The contour values are: 1.25, 1.75, 2.5, 3.75, 5, 7.5, 10, 12.5, and 15 mJy/synthesized beam. **c** Contours showing the percentage polarization on a radio photograph of 1004+34

**Table 3.** Background sources near the lobes of 3C236

| Source | Measured position (1950.0) | | Flux densities (mJy) | | | Identification |
|---|---|---|---|---|---|---|
| | RA | Dec | $S_{49}$ | $S_{21}$ | $S_6$ | |
| A | $10^h02^m21^s.27$ | 35°17'30".3 | - | 8.7 | - | none |
| B | 10 04 21.32 | 34 59 52.8 | - | 9.1 | - | $20^m$ BSO |
| C[a] | 10 04 28.89 | 34 59 16.7 | 155 | 95 | 107 | $22^m.5$ BSO? |
| E[b] | 10 04 47 | 34 53 29 | 130 | 60 | 20 | none |

[a] 6 cm observations show 20″ extensions in p.a. 20° about the strong nuclear component
[b] 6 cm observations show a 30″ double in p.a. 90°

less than 20%. This contrasts with the fact that in the central and northern portions the degree of polarization is almost always 30% or higher.

*c) 6 cm Wavelength*

We have observed both outer lobes of 3C236 with the WSRT at 6 cm (Table 1). In 1002+35 we detect no emission at full resolution, which means that no fine scale features smaller than about 4″ (6.5 kpc) have a flux density greater than 2 mJy ($6\,10^{22}$ W/Hz). After convolution to the 21 cm resolution, however, both the outer peak and the end of the inner ridge (at $RA = 10^h02^m15^s$, Dec = 35°16′) appear. Since the front edge of this inner peak is unresolved in the 21 cm map, its size must lie between 4″ and 15″ (6.5 and 25 kpc).

In the 6 cm observation of the outer part of 1004+34 we see emission from the leading edge, as well as peaks *C*, *D*, and *E*. At

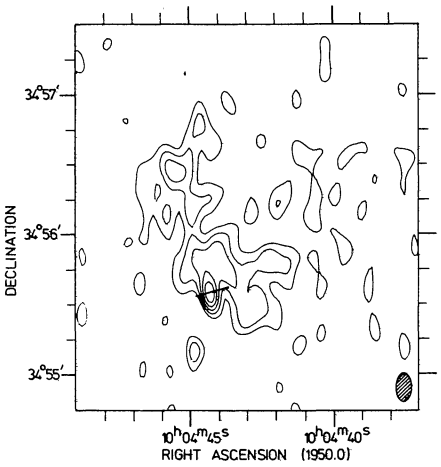


**Fig. 6.** A contour plot of the 6 cm map showing the leading edge (peak *D*) of 1004+34. Contour values are: −3 (dashed), 1.5, 3, 4.5, 6, and 7.5 mJy/synthesized beam. A short line, showing the electric vector position angle of the only polarization detected, has been drawn at the position of the 5.5 mJy polarized peak

$RA = 10^h04^m44^s.3$, Dec = 34°55′36″, partially embedded in diffuse emission from the outer edge, lies a compact, highly polarized "hot spot" (Fig. 6), the core of peak *D*. The adjacent structure makes it difficult to determine the size of this feature although there is evidence that it is partially resolved in declination. We estimate that its narrow dimension can be no more than about 4″ (or 6.5 kpc), while its flux density (which may include a contribution from the diffuse emission) is 9.6±1 mJy. At the same position (to within 1″) we measure 5.5±0.7 mJy of linearly polarized flux in position angle 106°±4°. This polarized emission, which is unresolved, corresponds to a degree of polarization for the hot spot of 57%±10%.

When convolved to the 21 cm resolution, the flux density of the peak increases to about 40 mJy while the polarized flux remains constant (5.2±1.3 mJy), so there is a corresponding decrease in the degree of polarization to 13±3%. Since this value agrees with that found at 21 cm (Fig. 5c) we conclude that most of the polarized flux arises in the hot spot, the surrounding diffuse emission being not more than 20% polarized.

Both peaks *C* and *E* are resolved at 6 cm (information about their structure is given in Table 3). The inverted spectrum apparent in the flux densities of *C*, presumably caused by the compact nuclear component, and its identification with a blue object suggest that it may be a quasar.

## 4. Source Properties as a Function of Wavelength

We have intercompared the multifrequency spatial distribution of total intensity and polarized radiation from 3C236 in a manner analogous to that used in Paper I. The main uncertainties in the analysis of 3C236 arise because a) there are hardly any single dish observations to which we can relate our aperture synthesis data; and b) there are serious residual dynamic range effects which influence the 21 cm maps, especially when convolved to the 49 cm resolution. Another serious problem is that the angular size of 3C236 is comparable to the WSRT 21 cm primary beam half power width. Since the telescopes were pointed at the nuclear source, the outer edge of 1004+34 is 24′ from the field center. Due to limitations in the pointing accuracy, the primary beam correction in this region is uncertain by about 10% which may produce systematic spectral index errors of ±0.1. (The problem of off-axis instrumental polarization was discussed in Sect. 2.)

**Table 4.** Measured source parameters for 3C236

| | RA (1950.0) | Dec (1950.0) |
|---|---|---|
| Radio position of nuclear source[a] | $10^h03^m05^s.38 \pm 0^s.08$ | $35^o08'48''.2 \pm 1''.0$ |
| Relative offset of optical galaxy (arc s) | +0.6 | +0.5 |

| | 1002+35 | 1004+34 | Nuclear source | Integrated |
|---|---|---|---|---|
| $S_{49.2}$ (Jy) | 1.94±0.10 | 1.35±0.07 | 5.06±0.10 | 8.35±0.27 |
| $S_{21.2}$ (Jy) | 0.97±0.10 | 0.72±0.05 | 3.20±0.10 | 4.89±0.25 |
| $S_{6.0}$ (Jy) | - | - | 1.29±0.10 | - |
| Spectral index, $\alpha$[b] | -0.82±0.14 | -0.75±0.10 | -0.66±0.05 | -0.64±0.07 |
| % $Pol_{49.2}$ | 7.3 ±0.9 | 6.4 ±0.8 | <0.2 | (1.3 ±0.2) |
| Position $angle_{49.2}$ | 66 ±2 | 131 ±1 | - | (85 ±5) |
| % $Pol_{21.2}$ | 12.5 ±2.9 | 6.0 ±2.1 | <1 | (2.4 ±0.6)[c] |
| Position $angle_{21.2}$ | 42 ±2 | 56 ±5 | - | (40 ±7)[c] |
| % $Pol_{6.0}$ | - | - | <2 | - |
| Suggested RM (rad $m^{-2}$) | 2.2 | 6.6 | - | - |

[a] Mean of 6 cm observations of the nucleus and 3C 236 (west)

[b] $\alpha$ defined as $S \propto \nu^{\alpha}$. For the nuclear source the error in $\alpha$ is based solely on the least squares fit

[c] Including Baker's (1974) polarization for the nuclear source

### *a) Spectral Index Variations*

We computed the spectral index distribution between 49 cm and 21 cm after convolving the latter data to the former's resolution. A one dimensional cross cut along the major axis (position angle 122°.5) through the spectral index map is shown in Fig. 7.

With the 49 cm resolution the south following lobe, 1004+34, is barely resolved in its minor dimension so the cross cut in Fig. 7 gives essentially all the information about its spectral index distribution. There appear to be no significant spectral index variations in 1004+34. Although we have not plotted spectral data for the faintest part of the tail where the signal/noise ratio is low, direct comparison of the 49 cm and 21 cm data indicates a constant spectral index of about −0.75 to the east of $10^h03^m36^s$. This corresponds to a distance along the lobe of about 16′ (1.6 Mpc).

The situation in 1002+35 is more complex. The cross cut through the convolved 21 cm map (Fig. 7) shows a serious negative residual near the central source which remains despite our various attempts (Sect. 2) to minimize instrumental defects. Its presence produces large uncertainties in the spectral index distribution of the lobe to the east of $10^h02^m38^s$. Figure 8 shows the spectral index map west of this location. Typical errors in $\alpha$ are ±0.08 so we have chosen a contour interval of 0.1. The peak in the polarized emission near $RA = 10^h02^m6$, Dec = 35°13′.5, which lies close to a region (unresolved at 49 cm resolution) where the spectral index flattens abruptly, is the only possible correlation between a spectral index variation and a feature in the observed radio emission.

Are the spectral variations seen in Figs 7 and 8 real? Some occur on sharp gradients in the total intensity distribution (e.g.,

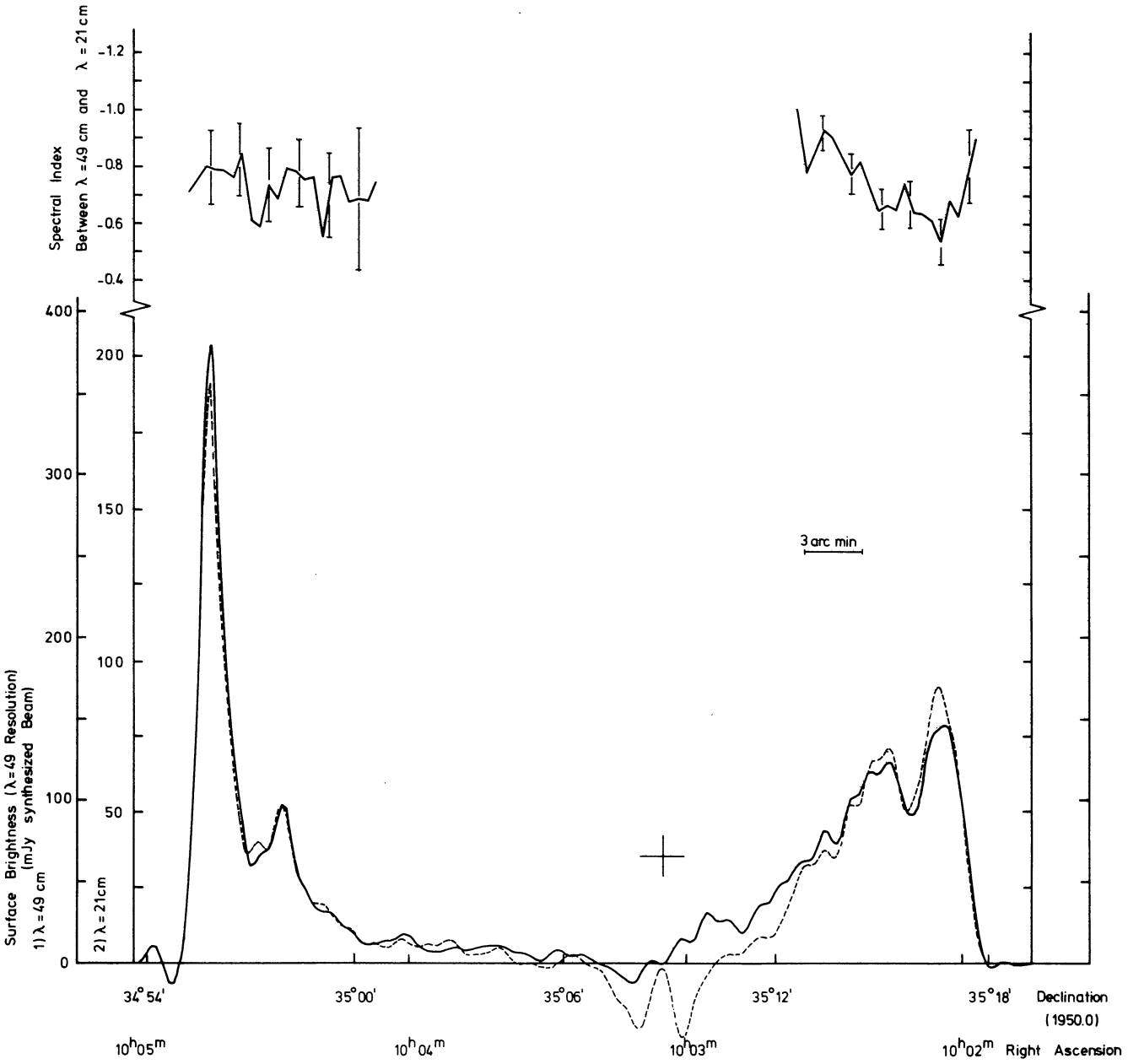


**Fig. 7.** Crosscuts along the major axis of 3C236 showing at the bottom the total intensity distribution in the outer components at 49 cm (solid) and 21 cm (dashed). A cross indicates the position of the central source, which has been subtracted off. The spectral index distribution along each component is shown above, with bars indicating errors based on the uncertainties in the two measurements

the outward steepening at the leading edge of 1002+35 seen in both Figs. 7 and 8). Spectral indices computed along such steep gradients can be notoriously unreliable if, a) despite our attempts to produce maps with identical gaussian beams, different relative amounts of flux were affected by the Clean procedure at the two wavelengths; or b) flux is missing from either map. While possibility a) is difficult to check, b) could be important for 1002+35.

If we compare the integrated flux densities obtained at 21 cm for 1002+35 and 1004+34 with single dish values (Bridle et al., 1972; the contribution of adjacent background sources has been included in our flux densities for the purpose of the comparison), we find good agreement for 1004+34, but in 1002+35 our measurement is about 20% low. This suggests that the interferometer measurement may indeed be missing some flux. Further support for this conclusion comes from 43 MHz observations of 3C236 made by Perley (1977) with the University of Maryland's Clark Lake Telescope. Perley has measured the relative flux of the two components and the value he gets is in good agreement with that expected from an extrapolation of the Bridle et al. 21 cm flux densities and our 610 MHz integrated values (assuming the spectra are straight). Use of our 21 cm flux densities does not give satisfactory agreement.

As a check on the reality of the spectral variations seen in 1002+35 between 21 cm and 49 cm, it is clearly desirable to have a third high resolution map of 3C236 in this wavelength range. Note however that Perley does find most of the 43 MHz flux from the components located near their outer ends, observing no

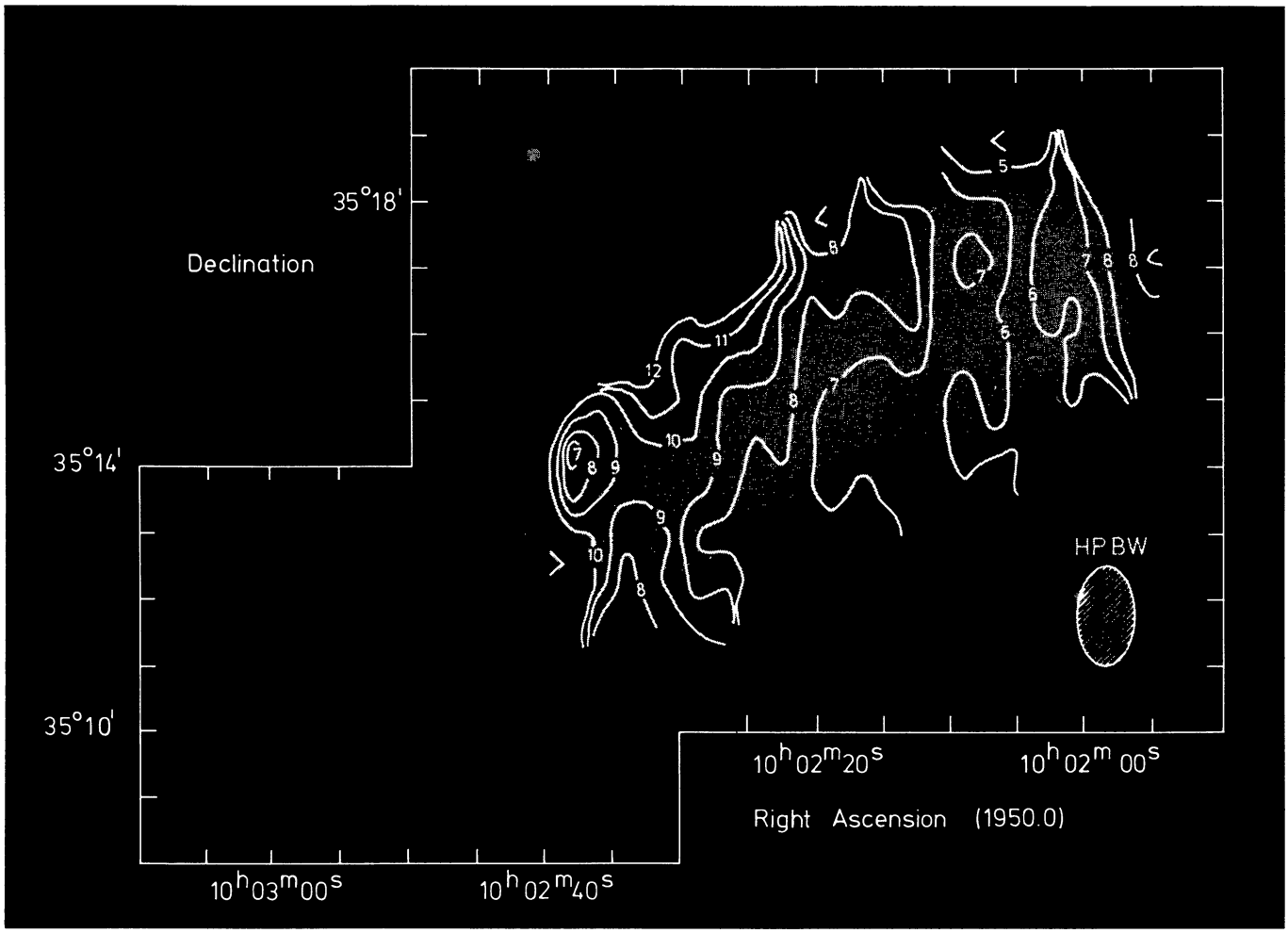


**Fig. 8.** The spectral index distribution in 1002+35, shown as contours of $\alpha$ (multiplied by $-10$), on a photograph of the 49 cm total intensity distribution. The spectral index was determined between 49 cm and 21 cm

brightening of the weak trailing emission compared to our 610 MHz map, which is consistent with the lack of spectral index variation we find in 1004+34.

At higher frequencies, however, there is significant evidence for a steepening of the spectrum in both components. Baker et al. (in preparation) have compared a smoothed version of the 49 cm map shown in Fig. 1 with a 6 cm single dish map. They find that in both components the spectrum steepens appreciably going from the bright outer heads along the weaker trailing emission. The pattern seen in 1002+35 is strikingly similar to that observed between 21 cm and 49 cm (Fig. 8). We conclude that the relative variation in spectrum seen in 1002+35 may indeed be unaffected by the flux missing at 21 cm, and that in any event at wavelengths shorter than 21 cm the spectrum found in the weak trailing emission of both components does steepen.

Our 6 cm observations suggest that the spectrum of the bright outer head (Peak *D*) of 1004+34 may flatten with decreasing wavelength. The 49–21 cm spectral index of the peak is $-0.79\pm0.13$ (Fig. 7). Convolving the 6 cm map to the 21 cm resolution (Fig. 9) gives a spectral index of $-0.60\pm0.11$, and further convolution to the 49 cm resolution gives a 49−6 cm spectral index for the peak of $-0.68\pm0.04$. While the changes by themselves are only marginally significant, other facts suggest that they are likely to be real.

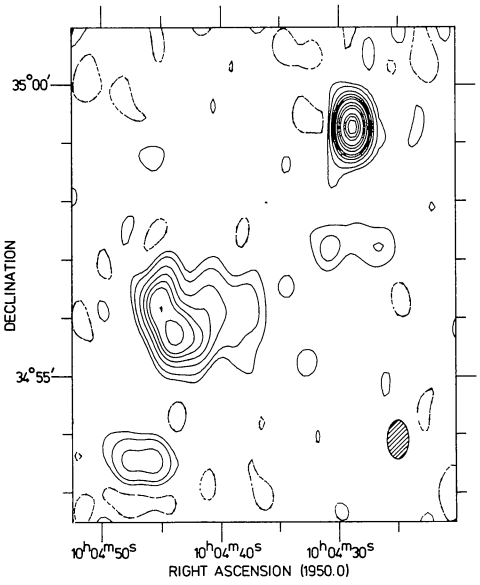


**Fig. 9.** The 6 cm observation of 1004+34, convolved to the 21 cm resolution. Contour values are: $-2.5$ (dashed), 2.5, 5, 10, 15, 20, 25, 35, 45, 55, 75, 85, and 95 mJy/synthesized beam

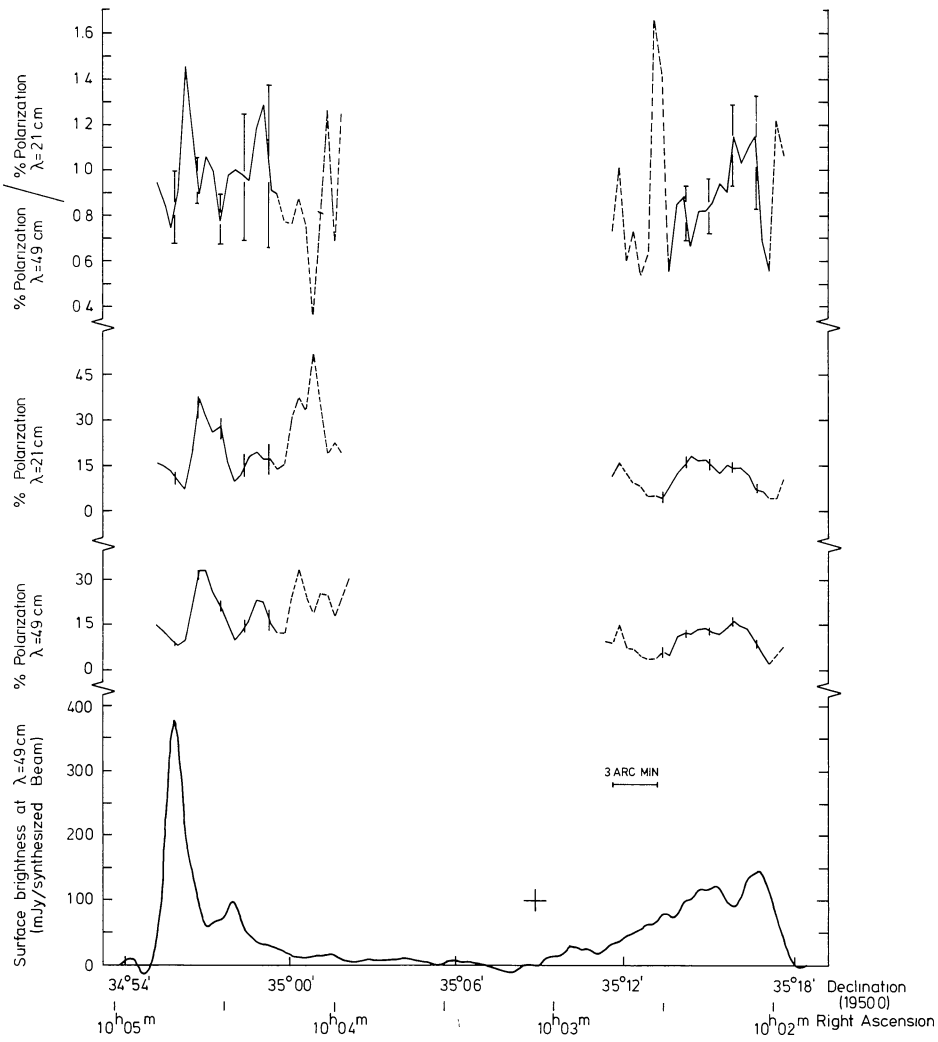


**Fig. 10.** Crosscuts showing polarization properties along the components of 3C236. At the bottom, for reference, is the 49 cm total intensity distribution. Above it are shown the 49 cm and 21 cm percentage polarization (made with the same resolution). The top graph shows the depolarization ratio. Typical errors are indicated by bars, and where the values become more uncertain a dashed line has been used

The 49, 21, and 6 cm observations of peak *E* (Table 3) give values consistent with a straight spectrum having $\alpha = -0.89$. This is good evidence that uncertainties such as pointing errors affecting the 21 cm data far from the field center are not systematically biasing the data.

Our 6 cm observation, because of its sampling increment of 36 m, is increasingly insensitive to structures exceeding about 3′. This is apparent in that emission from the tail behind peak *D* is absent from the convolved 6 cm map (such emission would, in fact, fall below the lowest contour plotted in Fig. 9, but is also not present in much deeper contour plots). However, since this would have the effect of lowering the 6 cm flux, it would lessen the flattening of the spectrum discussed above rather than enhance it.

We thus conclude that there probably is a flattening of the spectrum of the outer head of 1004+34 between 6 cm and 21 cm compared with the 21–49 cm spectral index. A similar spectral flattening was seen in the bright head of the western component of 3C326 (Paper 1).

*b) The Polarization Data*

Polarization measurements at several wavelengths are a potential treasure-trove of information about a radio source: Variations in the degree of linear polarization depend on the density of thermal depolarizing plasma and magnetic field strength (Burn, 1966), while changes in the measured position angle [p.a. $= \frac{1}{2}\tan^{-1}(U/Q)$] can be used to extract the direction of the projected magnetic field. Derivation of the former is less ambiguous than of the latter, though its interpretation is more model dependent. Figure 10 shows a comparison between the 49 and 21 cm degrees of polarization, while for 1002+35, which has some two-dimensional structure, we also present a depolarization map (Fig. 11).

Both figures indicate that there is little or no depolarization in the outer lobes of 3C236 between 21 and 49 cm. The typical rate of depolarization in 1002+35 is about 0.9, though there are regions where no depolarization occurs (Fig. 11). On average, 1004+34 does not depolarize at all, a fact also reflected in its integrated polarization percentages (Table 4). On the other hand, the integrated polarization of 1002+35 drops substantially between 21 and 49 cm, but this is not necessarily inconsistent with the near absence of depolarization indicated by the distributed values. A large scale change in RM over the component (see below) is the likely cause.

We know of no polarization measurements of the outer lobes of 3C236 reported in the literature, which seriously hampers our ability to determine the rotation measure (RM) from our measurements. However, Reich has kindly made available some 11 cm measurements done with the Effelsberg 100 m telescope, from

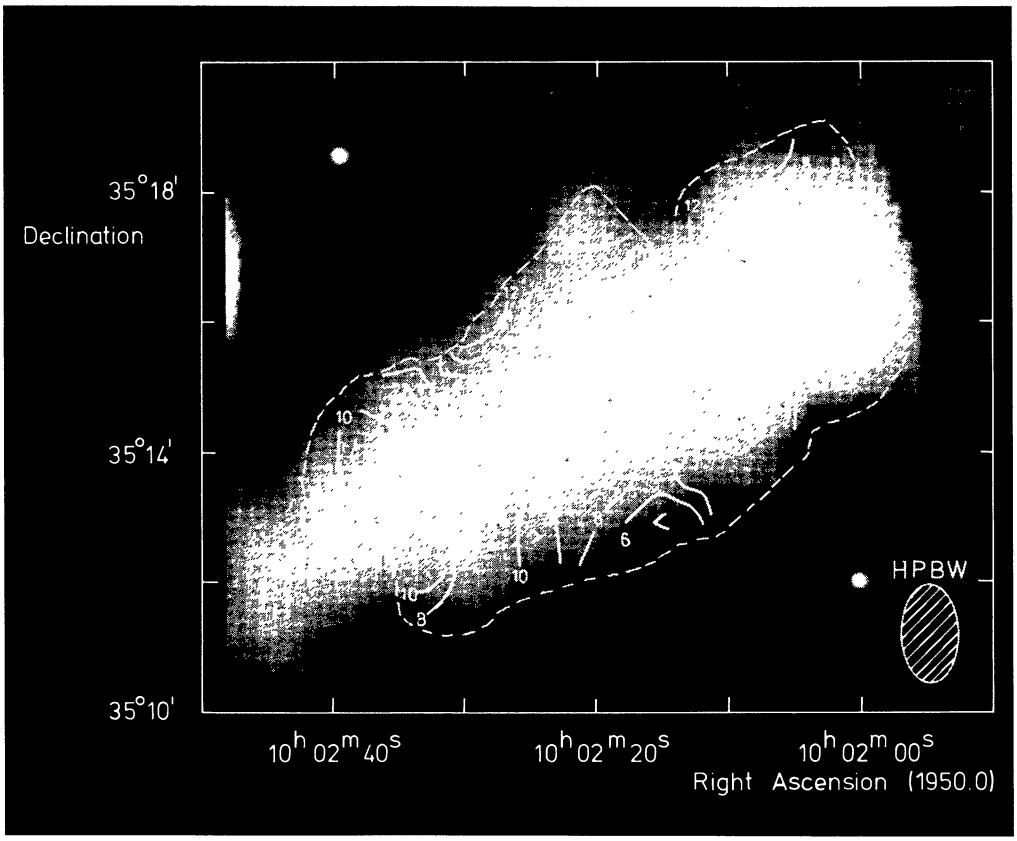


**Fig. 11.** The depolarization ratio in 1002+35, shown as contours of 10 times (49 cm percentage polarization/21 cm percentage polarization) superimposed on the 49 cm total intensity distribution. Numerous maxima (>) and minima (<) have been marked

which we have obtained integrated values for the position angle of the electric vector measured in 1002+35 (p.a. = 55°) and 1004+34 (p.a. = 51°). Noting that the values obtained are somewhat more uncertain than usual, Reich estimates the error to be between 10° and 20° (we shall adopt a value of ±15°).

Our attempts to deduce the RM and thereby intrinsic p.a. for each lobe have proceeded as follows:

(i) 1004+34

We have 49, 21, and 6 cm observations of polarized emission from peak *D* in this lobe. Those at 6 cm indicate that most of the polarized flux comes from the "hot spot" seen in Fig. 6, which is also supported by the other two measurements. From the p.a. determined at the polarized peak in each of the three maps, we find that a RM of either 9.5 or 23.6 rad m$^{-2}$ fits the data well (the former giving a slightly better least squares fit). If we now examine the integrated 21 and 49 cm data (Table 4) we find that they correspond to values of 6.6 and 22.6 rad m$^{-2}$, respectively, and would then expect the p.a. at 11 cm to be either 44° or 14°. The former is clearly in much better agreement with the p.a. measured at 11 cm (51°±15°), so we conclude that the average RM of 6.6 rad m$^{-2}$ is correct.

We have calculated the distributed RM from our 49 and 21 cm data, assuming there are no sharp changes within one half beamwidth. Figure 12a shows the resulting distribution relative to the average RM of 7 rad m$^{-2}$. The values calculated have in turn been used to derive the intrinsic p.a., and hence the magnetic field distribution, Fig. 12b. The field runs parallel to the major axis of the lobe, apparently following several wiggles in the total intensity distribution, but abruptly turns by 90° along the leading edge.

(ii) 1002+35

For this component the only WSRT polarization measurements are those made at 49 and 21 cm. However, we have reason to believe that the RM is probably small: Other extragalactic sources in this direction indicate that the contribution from the galactic foregound is minor (Spoelstra, private communication), in agreement with what we found for 1004+34 above. Moreover, the virtual lack of depolarization in both components means that the magnitude of their internal rotation measures cannot be large: |RM| $\lesssim$ 3 rad m$^{-2}$. The smallest RM one obtains from the integrated polarization for 1002+35 (Table 4) is 2.1 rad m$^{-2}$. Combined with the 49 and 21 cm position angles this gives p.a. = 38° at 11 cm, somewhat outside the range expected from the 11 cm measurement (55°±15°), though within the upper limit of Reich's estimated error. (For 1004+34 we found the measured p.a. too large by 7°; if we apply this adjustment to 1002+35, we obtain the satisfactory value 48°±15°.) We conclude that the average RM of 1002+35 is probably 2 rad m$^{-2}$.

The distributed RM obtained from our 49 and 21 cm data has been plotted in Fig. 13a with the average value subtracted off. It is apparent that the RM increases as one moves from east to west, which is probably due to the galactic foreground: still further east, in 1004+34, the RM is at least 7 rad m$^{-2}$. Moreover we know from the depolarization (Fig. 11) that the internal |RM| must be small. If the gradient in Fig. 13a arose internally, we might expect some correlation between it and the depolarization distribution (Fig. 11), which an intercomparison of the two does not reveal. As in 1004+34, we have used the distributed RM and measured p.a. values to derive the projected magnetic field distribution, Fig. 13b. The field is directed along the major axis of

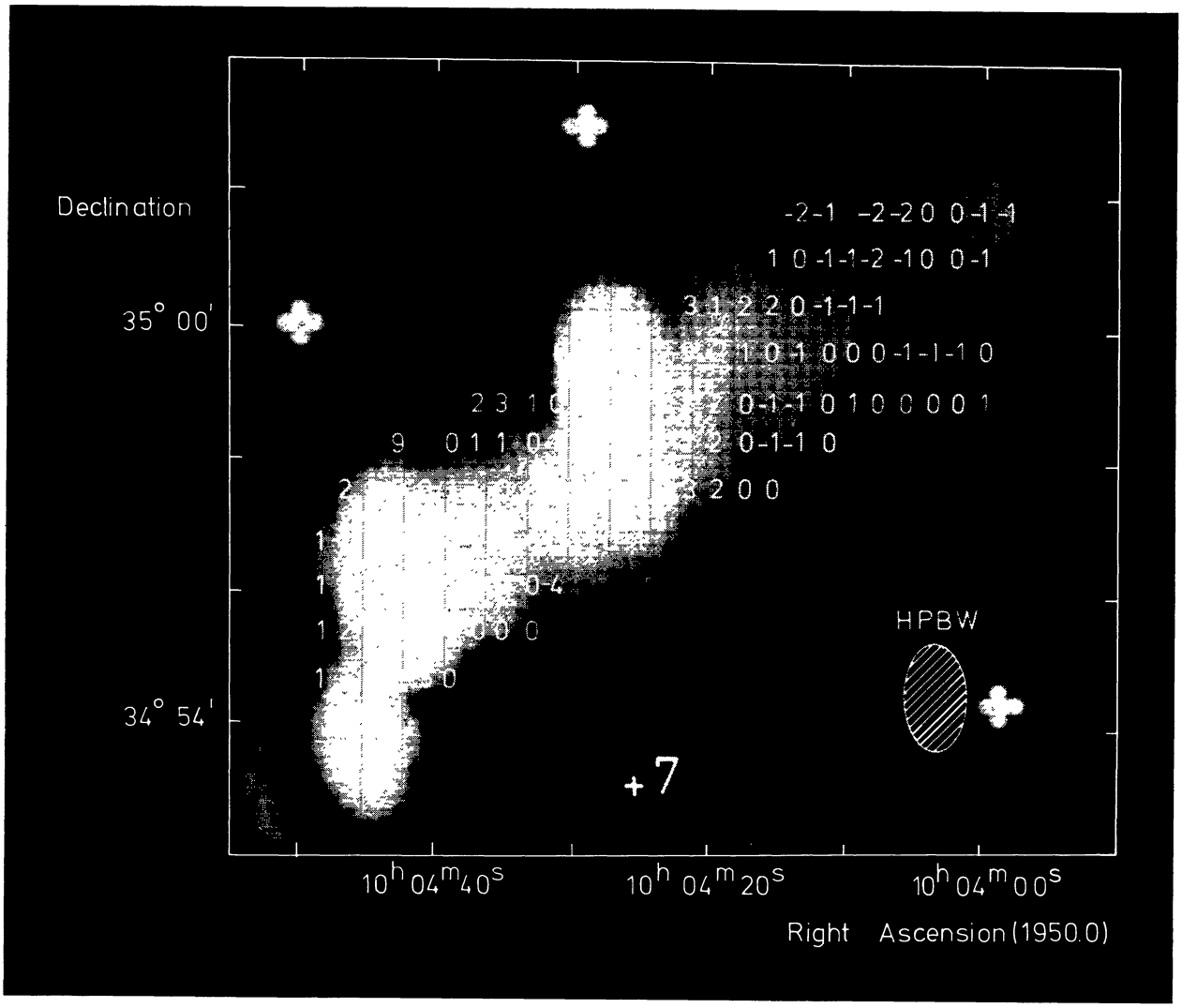


a

**Fig. 12a and b.** Rotation measure and magnetic field direction derived for 1004+34. **a** The most probable rotation measure distribution determined, as described in the text, from the position angles measured at 21 cm and 49 cm. Values of rotation measure, in rad m$^{-2}$, are shown with the mean of +7 rad m$^{-2}$ subtracted off. **b** The direction of the projected magnetic field derived using rotation measures shown in Fig. 12a. Each bar is orthogonal to the intrinsic electric vector determined at that point

the lobe, and as in 1004+34 abruptly turns to run tangentially along the front edge.

Since the variations in RM over both lobes are small, we can construct higher resolution maps of the magnetic field distribution from the 21 cm full resolution polarization maps (Figs. 4b and 5b). This has been done by applying to each lobe a correction corresponding to its average RM (an extra correction has been applied to the region of higher RM at the eastern end of 1002+35). The error thereby introduced in the resulting magnetic field distribution, Fig. 14a and b, should nowhere exceed 10°.

The increased resolution obtained in Fig. 14 reveals much more complexity, especially in the magnetic field of 1002+35. We see that along the edges of the lobe, the field appears to "flow" with the total intensity contours, following each wiggle and indentation. Near the outer edge, the field is directed along spurlike features in the total intensity distribution. In the region of the interior peak (near $10^h02^m.25$, 35°16′) there is evidence that the field has been distorted, its direction changing in accordance with the total intensity contours. At the northwest end of this feature, the abrupt change of field direction and drop in polarized intensity (Fig. 4b) suggest that the field may be tangential to the leading edge, as is the case at the outermost end of each lobe. In 1004+34, Fig. 14b shows that the change in field direction near the front edge is a relatively smooth transition, though it otherwise differs little from Fig. 12b.

## 5. Discussion

In the preceding sections we have presented and qualitatively discussed the primary data obtained from our 6, 21, and 49 cm observations of 3C236, as well as derived quantities such as the spectral index, rate of depolarization, rotation measure and projected magnetic field direction. We now examine the implications of our observations for current models of the development and evolution of radio sources, and their physics. We begin by deriving intrinsic properties of the radio lobes.

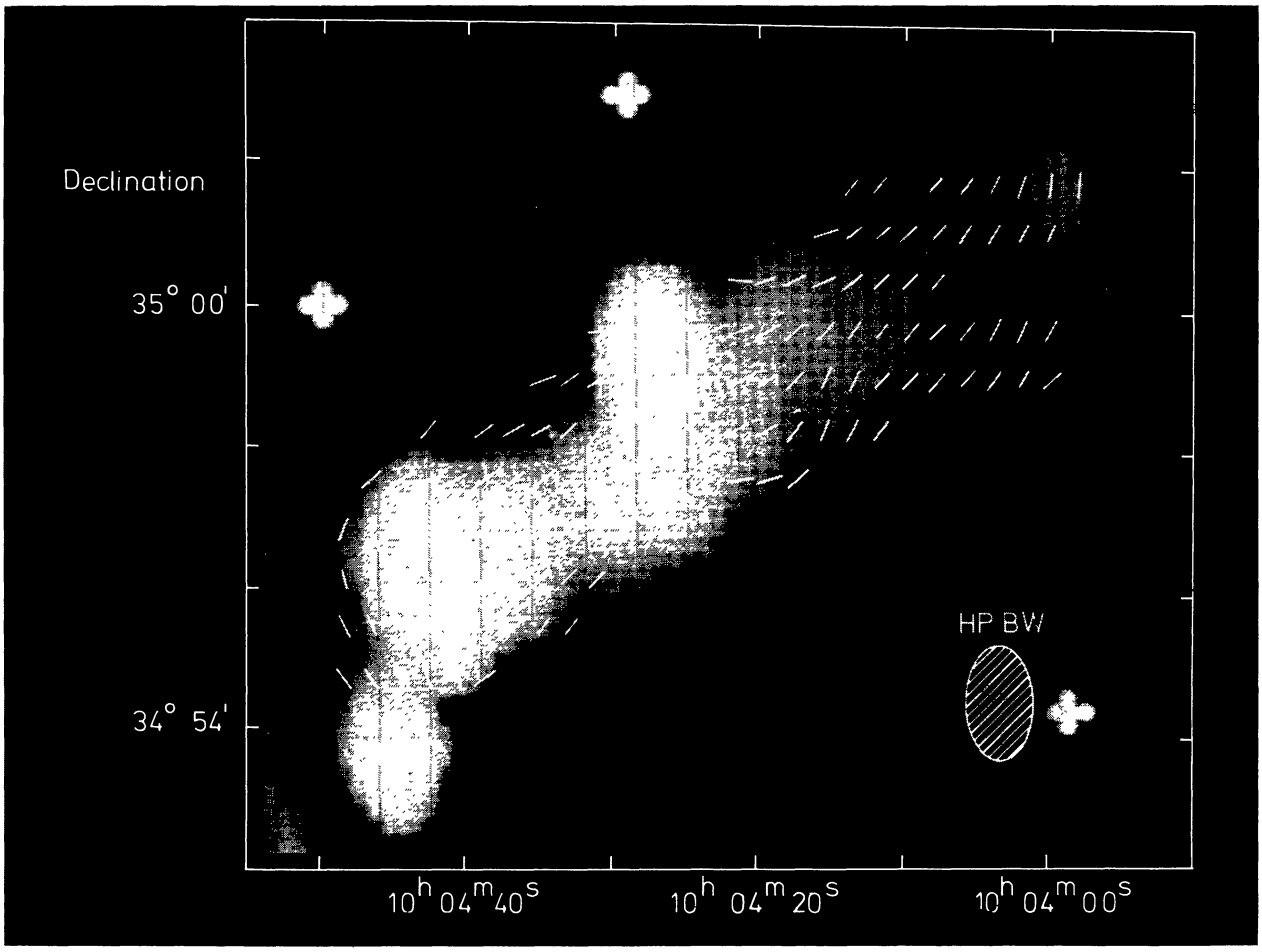


b

Distance and size data related to 3C236 are presented at the head of Table 5. The redshift is that of the elliptical galaxy which coincides with the central component (Sandage, 1967). Data presented for the individual components have been derived from the measured parameters (Table 4) using standard formulae (Pacholczyk, 1970). It must be emphasized that these are global parameters, indicating average conditions within each component. They will not be valid where deviations from the average are substantial, as in the hotspots: where necessary in our discussion, we will derive new values for such regions.

From the depolarization data (Figs 10 and 11), component sizes and equipartition magnetic field strengths (Table 5) we can use a simple model of depolarization by the large scale field within each component (Burn, 1966) to estimate the density of thermal electrons in the radio emitting region. Because the initial (short wavelength) depolarization rates for a variety of model configurations are similar, our estimate is relatively model insensitive. The values are shown in Table 6, where we have split 1004+34 into the brighter, more rapidly depolarizing head, and fainter tail region. From the density and magnetic field strength we can also calculate (or set limits to) the Alfvén speed in these regions, and the values are included in the table.

*a) Radio Source Models*

In Paper I we briefly discussed several current models for transporting energy from the central galaxy to the leading edge of the outer components. Here, as there, our observations are mainly indicative of what occurs after the energy is deposited in the outer lobe and throw little direct light on the energy transport mechanism. However, since the ultimate source of energy lies within the optical galaxy, we can note that as in 3C 326 there is excellent (though probably not exact) alignment between the outer components and the central nuclear source. The position angle of the great circle joining the hot spot in 1004+34 (Fig. 6) to the central source is $123^{\circ}0 \pm 0^{\circ}1$. This is approximately midway between the direction from the nuclear component to the inner and outer peaks ($124^{\circ}3 \pm 0^{\circ}3$ and $122^{\circ}1 \pm 0^{\circ}3$, respectively) seen in 1002+35 (Fig. 4a).

High resolution studies made of the central component (Fomalont and Miley, 1975; Fomalont et al., 1979) reveal double structure whose major axis has a position angle near 120°. The overall extent of this nuclear source, however, is some 2000 times less than that of the outer components. Since its spectrum is straight to 22.5 GHz its maximum age must be much less than that of the light travel time to the outer components (Fomalont et al., 1979). This interior double source, being clearly the result of more recent activity than that which produced the outer lobes, is direct evidence for a continuous, or quasi-continuous, flow of energy from the nucleus throughout the entire source's lifetime. The excellent alignment between inner and outer doubles indicates that the original expulsion orientation has been retained for a similar length of time (some $10^8$ yr if 1004+34 has travelled

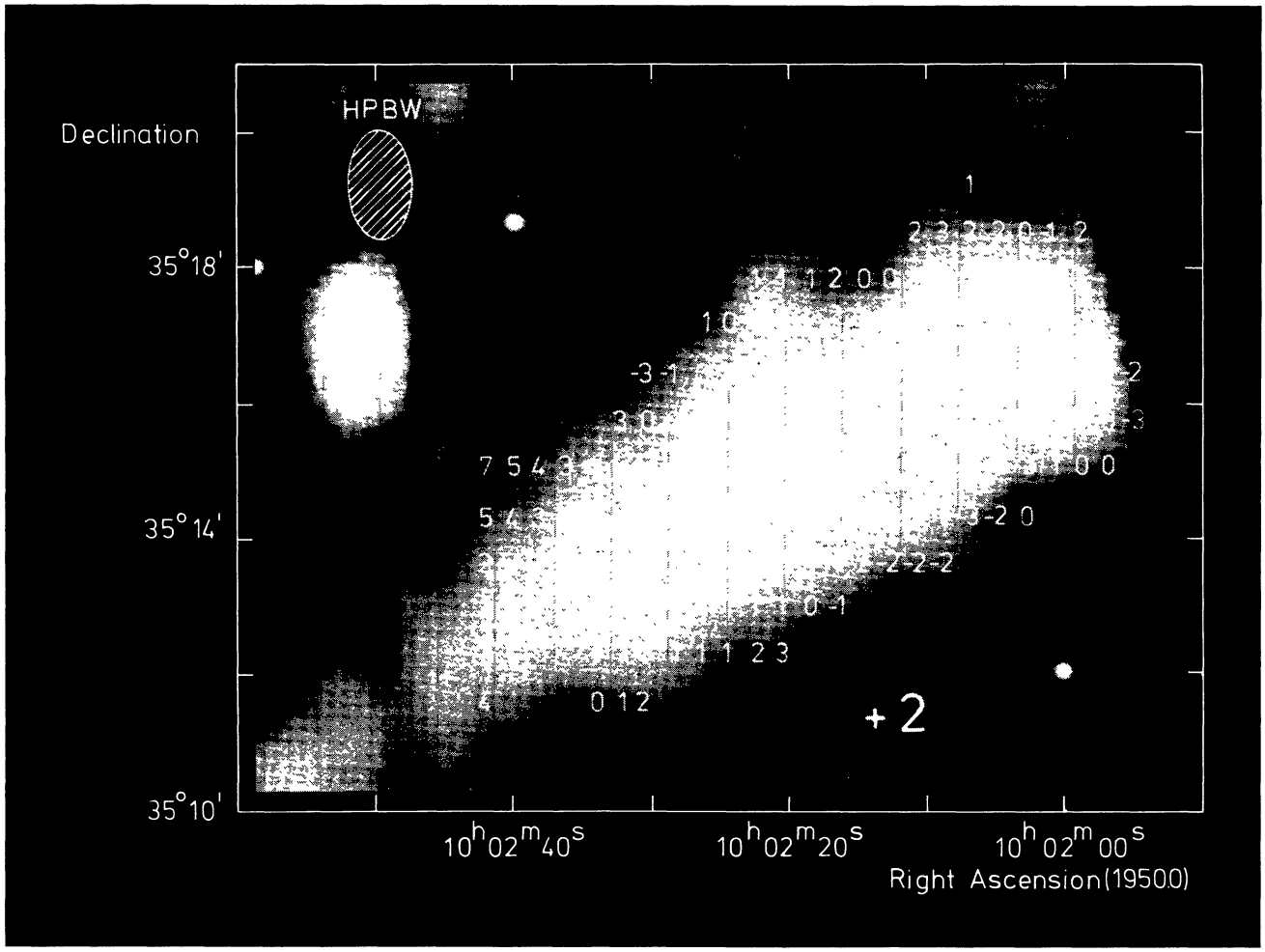


a

**Fig. 13a and b.** A likely distribution of rotation measure and magnetic field direction in 1002+35. **a** The rotation measure distribution derived, assuming the average value must be near that obtained for 1004+35, from the position angles measured at 21 cm and 49 cm (see text). The mean value of $+2\,\mathrm{rad\,m^{-2}}$ has been subtracted from each point. **b** The resulting projected magnetic field direction

at an average speed of $0.1\,c$ which, as we shall see below, is probably an overestimate). Morphologically and by way of radio spectrum, the components in the nucleus are indistinguishable from other double radio sources, and are probably simply the most recent set of secondary lobes.

A more striking example of a "secondary" component is the high brightness ridge immersed within 1002+35 which rises to a peak near $10^{h}02^{m}.25$, 35°16′ (see Fig. 4a). With the 21 cm beam this interior feature is the brightest part of 1002+35 and clearly has the morphological hallmarks of a radio component in its own right. From its position within the component, compactness and relative brightness we can be fairly certain that it was produced after the initial event which gave rise to the outermost emission from 1002+35. Further supporting evidence for this comes from the distortion in the magnetic field structure along the outer part of its leading edge (Fig. 14a) which was pointed out in Sect. 4b.ii, and which suggests that the interior component has entered a preexisting radio emission region. Its presence enables us to infer several important facts about radio source components.

Most currently discussed mechanisms for producing double radio sources are based on the idea that the outer components have been built up by the supply to them of energy in a nearly continuous manner (a notable exception is the hypothesis that pairs of compact, massive bodies are flung out of the nucleus, which seems implausible in 3C236 considering the alignment of inner and outer doubles). We feel that the interior component of 1002+35 as well as the nuclear double confirm this hypothesis, providing direct, concrete evidence that the lobe has been built up from a succession of minor components which move out much like the lobes themselves but carry only a fraction of their energy. (Of course we cannot reject the possibility that the interior lobe has itself been gradually built up by a continuous supply of energy.) Since none of the previous secondary components appear as discrete entities near or in front of the leading edge of 1002+35, they must have subsequently broken up and deposited their energy somewhere in this region.

The interior radio feature's minimum energy content is nearly $10^{57}$ erg, several hundred times less than that of the entire component (Table 5). Hundreds, perhaps thousands, of similar events must have preceded it if the scenario sketched above is correct, each supplying the lobe with less than 1% of its present energy. The discrete nature of the object presently seen in 1002+35 (for example, the way it has apparently modified the adjacent magnetic field structure) as well as its morphology suggest that it may be ram pressure confined. We now investigate the consequences of this possibility.

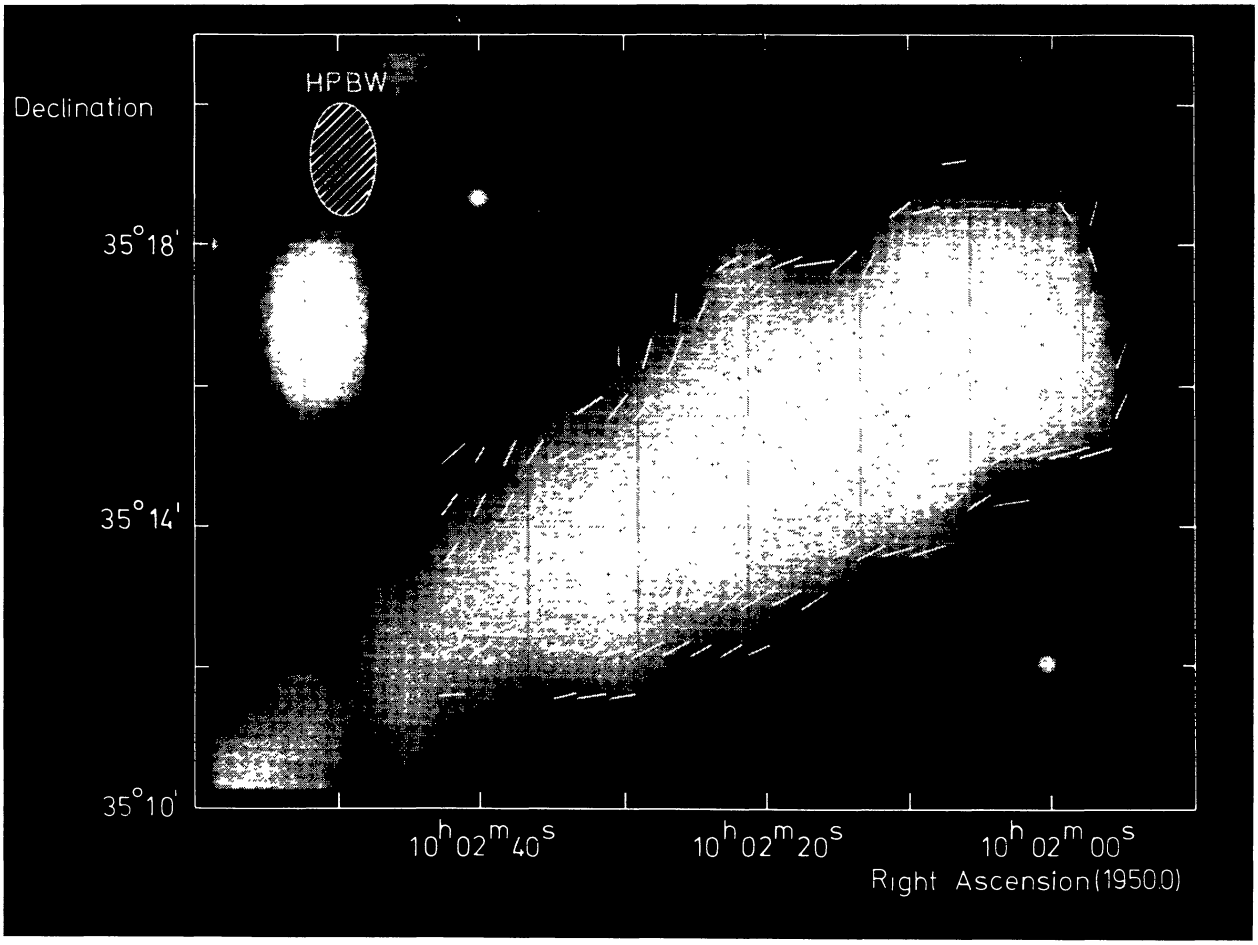


b

A plasma cloud expelled at a velocity $v_e$ into a medium of density $\varrho$ can be inertially confined by the ram pressure $\varrho v_e^2$ (Christiansen, 1969). Among the relationships one can derive is the expression,

$$\frac{d_0}{D}\varrho_c = \frac{3}{2}\varrho, \tag{1}$$

where $d_0$ is the component diameter when ejected, $D$ is the maximum distance the component will travel and $\varrho_c$ is its average density.

Usually one attempts to derive $\varrho$ from estimates of $D$, $d_0$, and $\varrho_c$. The situation in 1002+35 offers us a unique opportunity, in principle, to test Eq. (1) as the component's polarized emission should enable us to estimate both $\varrho$ and $\varrho_c$. Unfortunately, for the reasons detailed above in Sects. 3c and 4b.ii, it has not been possible to directly measure polarized emission from the interior lobe, although we have indirect evidence that it is polarized.

What we can do, however, is note that if the component is confined, then the internal and external pressures must balance. The former is determined by the component's internal energy density, $U_c$, while ram pressure and the external energy density, $U$, provide the latter. We have, therefore

$$U_c = U + \varrho v_e^2. \tag{2}$$

Using the generalized sound speed for the external medium, $v_s$ [$=(U/\varrho)^{1/2}$, which is equivalent to the Alfvén speed when the magnetic field is greater than or equal to the equipartition value], and combining it with (2) we obtain the relationship,

$$v_e = v_s(U_c/U - 1)^{1/2}. \tag{3}$$

Equation (3) is instructive as it expresses the component speed in terms of the external sound speed and the ratio of internal to external energy densities.

If the component is to be ram pressure confined its speed must be fully supersonic, so $v_e/v_s$ probably should be at least 5, which requires a ratio of internal to external energy densities of at least 25:1. We note that since this is a general result, any such condensation within a radio emitting region must have a corresponding radio brightness contrast if it is to be ram pressure confined. From our 21 and 6 cm measurements of the end of the interior component in 1002+35 we estimate $U_c/U \cong 20$. This ratio may be higher, but by no more than about a factor of 2. Thus we have $v_e \cong 4v_s$ and for the equipartition case (Table 6) the interior component must be moving at about 1900 km s$^{-1}$.

At this speed the travel time from the nucleus is about $5\,10^8$ yr and, still assuming that the nuclear double represents the next generation of secondary components, some $10^8$–$10^9$ yr must separate each discrete subcomponent from its successor. If, as argued above, there have been nearly a thousand such events, the outer components must be at least $10^{11}$ yr old. These lifetimes all seem quite large, but there appear to be only two possibilities for significantly decreasing them: 1. The present speed is in fact much greater than 1900 km s$^{-1}$; or, 2. The average component speed is much greater than its present value.

**Table 5.** Some physical parameters of 3C236

| | | | |
|---|---|---|---|
| Redshift | 0.0988 (Sandage, 1967) | | |
| Luminosity distance ($H_0$ = 75, $q_0$ = 0.5) | 365 Mpc | | |
| Angular extent | 40' | | |
| Projected linear extent | 3.9 Mpc | | |
| Size conversion ratio | 1.62 kpc arc $s^{-1}$ | | |
| | 1002+35 | 1004+34 | Nuclear source |
| Major axis (kpc) | ∿1270 | ∿1530 | - |
| Minor axis (kpc) | ∿300 | ∿150 | - |
| Major axis position angle ($^o$arc) | 121 | 121 | - |
| Volume ($10^{72}$ $cm^3$)[a] | 1.8 | 0.5 | - |
| $P_{49.2}$ ($10^{25}$ W $Hz^{-1}$) | 3.7 | 2.6 | 9.6 |
| $P_{21.2}$ ($10^{25}$ W $Hz^{-1}$) | 1.9 | 1.4 | 6.1 |
| L, $10^7$ - $10^{10}$ Hz ($10^{42}$ erg $s^{-1}$) | 1.5 | 1.0 | 4.0 |
| $E_{min}$ ($10^{59}$ erg)[b] | 2.6 | 1.2 | - |
| $H_{eq}$ (μG)[b] | 1.2 | 1.5 | - |
| Energy density ($10^{-13}$ erg $cm^{-3}$) | 1.5 | 2.2 | - |

[a] Calculated assuming each component is a prolate spheroid

[b] Equipartition parameters, calculated assuming that the energy contained in protons equals that of the relativistic electrons, and using the spectral indices in Table 4

**Table 6.** Approximate values derived from the 21–49 cm depolarization

| | 1002+35 | 1004+34 (tail) | 1004+34 (head) |
|---|---|---|---|
| Intrinsic degree of polarization (%) | 12 | 22 | 11 |
| Line of sight uniform component of magnetic field (μG) | 0.3 | 0.5 | 1 |
| Depolarization between 21 and 49 cm | 0.9 | 1.0 | 0.83 |
| Assumed line of sight depth through source (kpc) | 300 | 150 | 130 |
| Thermal electron density ($cm^{-3}$) | $4 \times 10^{-5}$ | $<2.5 \times 10^{-5}$ | $4 \times 10^{-5}$ |
| Alfvén speed (km $s^{-1}$) | 420 | >650 | 1600 |
| Total mass ($M_\odot$) | $6 \times 10^{10}$ | $<10^{10}$ | $1 \times 10^{8}$ |
| Internal \|RM\| (rad $m^{-2}$) | 2 | 1 | 2 |

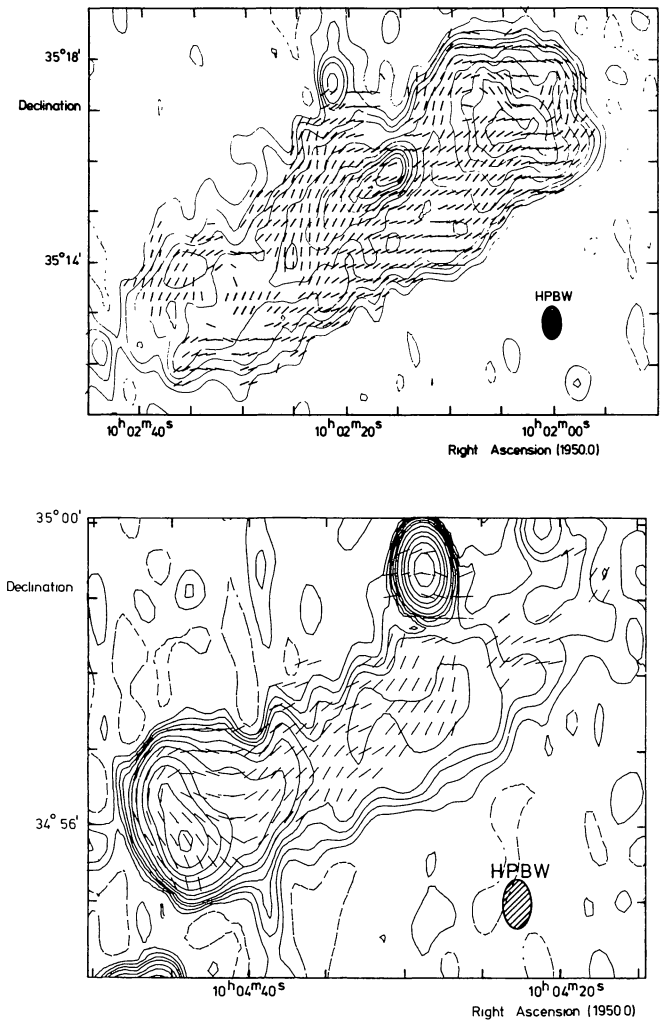


**Fig. 14a and b.** Magnetic field structure shown with the 21 cm resolution. The directions indicated by the bars were obtained by correcting the 21 cm position angles for the rotation measures in Figs. 12a and 13a (see also text). Contours of the 21 cm total intensity distribution are also shown (Figs. 4a and 5a). **a** 1002+35. **b** 1004+34

We believe both of these possibilities to be unlikely. In order for 1 to be significant there must either be large deviations from energy equipartition or we have overestimated the density, $\varrho$. Since $v_s$ depends on the square root of both $U$ and $\varrho$ we are concerned with *very substantial* changes in these parameters, and we doubt that such deviations are likely in such an extended, relatively relaxed component. Further high resolution polarization measurements, especially at long wavelengths, would however be valuable as a check on our estimate of $\varrho$. Possibility 2 is unlikely on simple probabilistic grounds, as one has the greatest chance of observing the component at that speed where it spends most of its time.

We conclude that, provided future polarization measurements do not significantly alter our interpretation of the depolarization in 1002+35 as resulting from internal Faraday dispersion, the present speed of the interior component probably is of order $10^3$ km $s^{-1}$, and its travel time has been nearly $10^9$ yr. Moreover, the ram pressure produced by the external medium is probably sufficient to confine the subcomponent.

We conclude our discussion of 1002+35 by commenting that we discern no features in the very outermost portions of the component (west of $10^h02^m.2$) which are characteristic of a "hot spot". The entire region is an amorphous plateau of emission whose maximum radio brightness in our 21 cm map (Fig. 4a) is somewhat less than that of the peak in the interior feature. Since

the outer lobe has not dispersed in the time interval between successive secondary components, it must clearly be confined for much longer than $10^9$ yr. The greater radio brightness near the leading edge as compared with regions closer to the galaxy suggests that ram pressure may play a significant role.

Let us now turn to the other component, 1004+34, where the situation may be rather different. There certainly is a morphological contrast, for 1004+34 has a hot spot at its leading edge. In the context of current models of radio component formation, the hot spot could be variously identified with the tip of a relativistic beam, a supermassive object, or the point of interaction of a ram pressure confined plasmon with the external medium. Given the evidence discussed above for multiple outbursts in 3C236 and the well-known difficulties which the supermassive object expulsion hypothesis encounters in trying to explain collimated multiple ejection, we will not consider this model further. Since the relativistic beam hypothesis gives the most tenable explanation of hot spots in sources such as Cygnus A (Hargrave and Ryle, 1974), we will examine some consequences of its application to 1004+34.

Hargrave and McEllin (1975) have investigated how relativistic particles in a radio hot spot might provide the energy for radio emission from the weaker tail or bridge regions. Assuming that material is continuously supplied from the relativistic fluid in the head, they derive a relationship (using an adiabatic equation of state) between the velocity at which the head moves into the external medium, the relative cross sectional areas and energy densities of head and tail, and the rate with which material flows out of the head and into the tail. Applying this to the hot spot in 1004+34 (Fig. 6), and assuming the sound speed there is $0.03\,c$ (a value suggested by Hargrave and McEllin for other sources which does not contradict what little we know about the hot spot in 1004+34), we obtain a very uncertain value for the velocity of the hot spot of several thousand $\mathrm{km\,s^{-1}}$.

But what should we take as "the hot spot"? One might argue that it is the entire "head" region along the leading edge of 1004+34 referred to in Table 6. For this and various combinations of "head" and "tail" one obtains speeds typically in the range 1000–5000 $\mathrm{km\,s^{-1}}$. These are similar to the 1900 $\mathrm{km\,s^{-1}}$ found for the interior component in 1002+35. The tendency towards higher values in 1004+34 suggests one possible reason for the greater distance it has travelled from the central galaxy. However, we must again emphasize the considerable uncertainty in these derived velocities, their inevitable dependence on energy equipartition assumptions, and in the case of the hot spots the question of what volume of space might enclose the relativistic fluid assumed to be present.

If in both components relativistic particles diffusing from the regions of highest surface brightness (whether they have been deposited there by relativistic beams or some other mechanism) are responsible for emission from the weak tails, the fact that they must suffer radiation losses has consequences for the spectral indices we have determined. Suppose that most of the particles we now "see" were deposited by the most recent outburst. Then their age is nearly $10^9$ yr. With no reacceleration, the inevitable radiation losses will result in a bend in the spectrum at 1415 MHz after some $9\,10^7$ yr, and at 610 MHz after $1.3\,10^8$ yr (van der Laan and Perola, 1969).

Although there is marginal evidence for some spectral steepening along the length of 1002+35 (Sect. 4a), it and the constant spectral index of 1004+35 appear to be inconsistent with the time scales we have just derived. We therefore conclude that, as in 3C326 (Paper I), some form of reacceleration or injection of fresh particles must occur throughout the lobes, and apparently often without the immediate presence of a hot spot. One might also expect to find evidence for spectral steepening at frequencies above 1415 MHz, and a recent comparison of our 610 MHz data with Bonn 5 GHz measurements suggests that this is the case. These results will be presented and discussed in detail later (Baker et al., in preparation).

*b) Further Implications*

Let us now turn away from our discussion based on specific models of radio source production to more general topics. One of the striking features of 3C236 is the difference in both size and shape of its outer components. This asymmetry is mirrored, to a limited extent, in the structure of the compact central source (Fomalont et al., 1979; Schilizzi et al., 1979), which also basically consists of two components. Of these, the southeastern one is dominated by regions of compact, high brightness radio emission, while the northwestern lobe has a substantially lower peak radio brightness and its emission appears smoother. Unless this is pure coincidence, it suggests that the crude morphological features may be determined very early in the energy release mechanism, even while still within the confines of the optical galaxy.

As for the relative sizes of 1002+35 and 1004+34, we have already noted that there is marginal evidence that the present velocities in the latter may be higher than those in the former. However, we believe there may be a more direct indication of what has happened. The interior lobe in 1002+35 clearly lies north of the geometrical axis of the entire component (Fig. 4a), while the outer hot spot in 1004+34 is in the southern half (Fig. 5a). This arrangement, which may be a manifestation of the well-known *S*-symmetry in double sources, suggests that although the two brightest peaks do not line up perfectly with the central one (the three forming an angle of $178\overset{\circ}{.}7 \pm 0\overset{\circ}{.}3$, a fact we investigate further below), they were probably produced at about the same time. It is then clear that the average speed of one is at least twice that of the other; indeed the feature in 1002+35 has yet to reach the leading edge. And so it has probably been with all the secondary components, those in 1004+34 travelling faster, always pushing the leading edge out at a greater rate. Although the reason for this greater speed is unknown, it is tempting to speculate that it is due in part to the apparent initial relative compactness of the components on the southeastern side.

As we have tacitly assumed throughout this discussion, the components expelled from 3C236 move through, and interact with, an external medium. Eventually they will be brought to rest by that interaction, while the galaxy, if it was initially moving through the medium, will leave the lobes behind. (Because of its greater mass and smaller cross section the galaxy's interaction with the medium is negligible.) The near perfect collimation of 3C236 suggests that if there is an external medium, the galaxy is practically at rest in it.

Jaffe and Perola (1973) have considered the problem of a galaxy expelling components at a velocity $v_e$ perpendicular to its own velocity $v_g$. They derive a relationship [their Eq. (6)] which we can rearrange as:

$$\frac{v_g}{v_e} = \frac{-\tan\frac{\Theta}{2}}{1+\left(1+\frac{v_g^2}{v_e^2}\right)^{-1/2}\frac{D}{y}\ln\left(1-\frac{y}{y_m}\right)}, \tag{4}$$

where new variables are $\Theta$, the supplement of the angle formed by the two outer components and the central galaxy; $y$, the distance

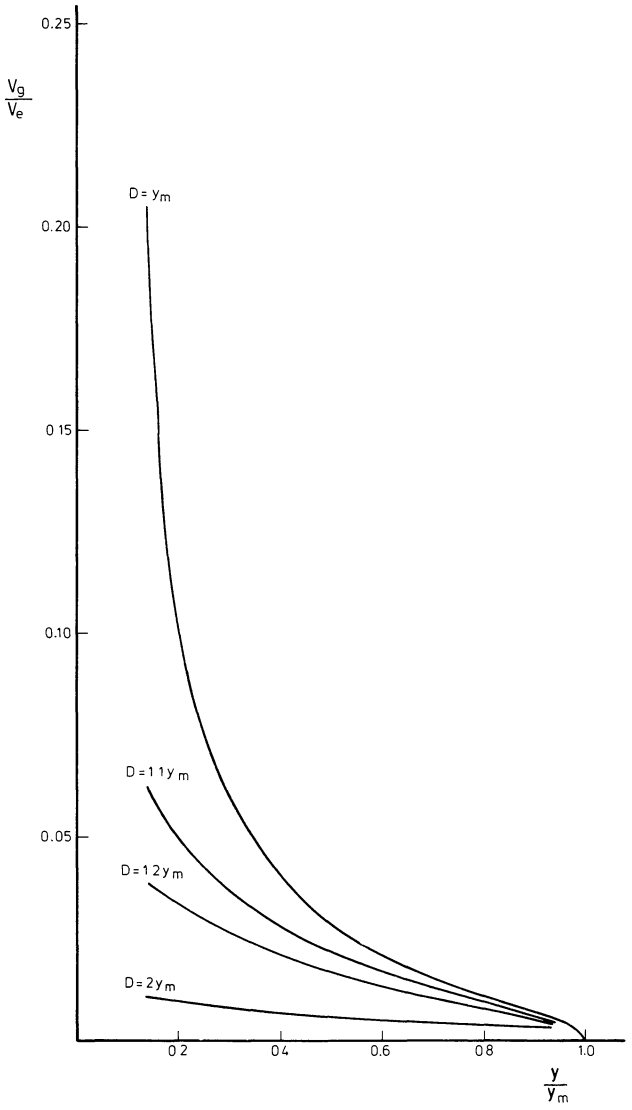


**Fig. 15.** Curves showing the ratio of the speed of the 3C236 galaxy, $v_g$, to the component expulsion speed, $v_e$ (where $v_g$ is assumed perpendicular to $v_e$), as a function of $y$, the lateral distance the components have travelled, expressed as a fraction of the lateral stopping distance, $y_m$ (for 3C236 we have taken $\Theta = 1\overset{\circ}{.}3$, see Eq. (4) and the accompanying text). We present this relationship for several values of $D$, the total component stopping distance

travelled by the component perpendicular to $v_g$; and $y_m$, the stopping distance in this direction ($y_m = D \sin\beta$ in Jaffe and Perola). Depending on the actual values of $y$, $y_m$, and $D$ (note $y \leqq y_m \leqq D$), we can estimate $v_g/v_e$ from $\Theta$. Although there must be an external medium (i.e. $\varrho > 0$) if we are to see any bending, it is noteworthy that $v_g/v_e$ does not depend on $\varrho$. Equation (4) takes no account of projection effects, which are probably negligible.

In order to evaluate Eq. (4) we need the relative values of $y$, $y_m$, and $D$. In Fig. 15 we show how $v_g/v_e$ depends on $y/y_m$ for various values of $D/y$, where we have taken $\Theta = 1\overset{\circ}{.}3$, the value one obtains by linking the brightest peaks in the outer components as discussed above. In view of the overall size of 3C236 it is unlikely that $y$ is very much smaller than $y_m$. Examining Fig. 15, we note that even if $y = 0.5\, y_m$ then regardless of the relative values of $D$ and $y_m$, $v_g$ must be less than $0.03\, v_e$, which is already a rather stringent limit. What value should we take for $v_e$? Clearly, it must exceed the present speeds which we have tried to estimate above. However, if $v_e$ is too large then the total component kinetic energy becomes excessive: If all the material in 1002+35 was expelled at a speed of 3000 km s$^{-1}$, its initial kinetic energy would exceed the present energy content by a factor of 10. To be conservative, let us suppose $v_e \leqq 10^4$ km s$^{-1}$. This means $v_g < 300$ km s$^{-1}$, which is so low that it suggests the 3C236 galaxy may be essentially at rest with respect to the external medium, a result whose implications we will now consider.

The 3C236 galaxy falls exactly on the Hubble relationship for radio galaxies (Sandage, 1972), so it probably has properties similar to those of first-ranked cluster galaxies. Consequently its mass, according to Sandage, is likely to lie between $10^{12}$ and $10^{13}\, M_\odot$. The mass of the radio components estimated from our polarization measurements (Table 6) is about $6\,10^{10}\, M_\odot$, which supports Sandage's suggestion since the components presumably contain only a small fraction of the total mass. There is, however, no indication of a cluster in the vicinity (e.g. Zwicky and Herzog, 1966). Wyndham (1966) notes the presence of several faint objects to the north, but these notwithstanding 3C236 appears to be isolated. This is at least consistent with the low densities in the vicinity of the radio lobes suggested by both their exceptional extent and small internal densities.

From this we conclude that 3C236 is associated with a very massive elliptical galaxy which lies nearly at rest in a region where the density of intergalactic material is extremely low. It has been suggested that the gas initially present in elliptical galaxies must have been stripped from them at an early stage, either by interaction with other galaxies or through external winds. It seems to us that in the case of 3C236 this hypothesis can only be maintained if we assume that its galaxy has devoured all other galaxies in the vicinity and/or accumulated the gas originally present. Since it is unlikely that every single neighbouring galaxy could have been removed, further optical work, especially to determine the nature of the faint objects to the north, would be desirable. Moreover, if the galaxy has accumulated much gas in its deep gravitational potential, this material is likely to be very hot and thus emit X-rays. Observations with the new generation of X-ray telescopes should set useful upper limits to the amount of hot gas actually present, if not detect it.

Finally, we turn briefly to a different aspect of the immense size of radio sources such as 3C236, the fact that the scale of their magnetic fields can set stringent limits to the mass of the photon (Goldhaber and Nieto, 1971). A massive photon implies a well known frequency dispersion in the velocity of light (one of the classical tests for this phenomenon). By the same token, it produces exponential decay in a static field over a distance $r$:

$$H = H_0 \exp(-\mu r), \tag{5}$$

where $\mu$ is the photon mass in terms of wave number (Goldhaber and Nieto, 1971). The presence in sources like 3C236 of magnetic fields extending over 1 Mpc and more would then seem to imply $\mu < 3\,10^{-25}$ cm$^{-1}$ which is some 14 orders of magnitude lower than the best terrestrial limit. Although this is the minimum lower limit we can expect from static fields, such a blind application of Eq. (5) is probably unrealistic (see Goldhaber and Nieto, 1971). As we discuss elsewhere (Strom and Willis, in preparation), more realistic estimates can readily set limits $10^7$ times smaller than terrestrial values, corresponding to a mass less than $4\,10^{-55}$ g.

## 6. Conclusions

From our observations of the extended outer components of 3C236 we have been able to derive fairly detailed information about the distribution of such parameters as the spectral index, minimum energy density and magnetic field structure. We find evidence for the presence of two generations of secondary components in the source, which we interpret as the mechanism by which energy is supplied to the outer lobes at intervals of $10^8$–$10^9$ yr. This supports the often-stated view that radio components are energized continuously or quasi-continuously throughout their lifetimes, and we find the present secondary components to contain somewhat less than 1% of the (minimum) energy of the outer lobes.

The near-perfect alignment between the nuclear component and outer lobes enables us to put stringent limits on the speed of the central galaxy through the surrounding medium. This, together with the nearly empty optical field, has implications for the formation of the 3C236 galaxy which appears to be a massive elliptical. Finally, we note that the presence of large scale magnetic fields in giant radio galaxies like 3C236 can set significant upper limits to the mass of the photon.

*Acknowledgements.* We wish to thank a number of colleagues, especially Drs. C. A. Norman, R. D. Ekers, and J. G. Robertson, for helpful discussions. We are grateful to Dr. W. Reich for providing unpublished Effelsberg measurements. The Westerbork Radio Observatory is operated by the Netherlands Foundation for Radio Astronomy with the financial support of the Netherlands Organization for the Advancement of Pure Research (Z.W.O.).

## References

Baker, J.R.: 1974, *Mem. Soc. Astron. Ital.* **45**, 579
Bridle, A.H., Davis, M.M., Fomalont, E.B., Lequeux, J.: 1972, *Astron. J.* **77**, 405
Burn, B.J.: 1966, *Monthly Notices Roy. Astron. Soc.* **133**, 67
Christiansen, W.: 1969, *Monthly Notices Roy. Astron. Soc.* **145**, 327
Christiansen, W.N., Högbom, J.A.: 1969, Radiotelescopes, Cambridge University Press
Fomalont, E.B., Miley, G.K.: 1975, *Nature* **257**, 99
Fomalont, E.B., Miley, G.K., Bridle, A.H.: 1979, *Astron. Astrophys.* **76**, 106
Goldhaber, A.S., Nieto, M.M.: 1971, *Rev. Mod. Phys.* **43**, 277
Hamaker, J.P.: 1978, *Radio Science* **13**, 873
Hargrave, P.J., Ryle, M.: 1974, *Monthly Notices Roy. Astron. Soc.* **166**, 305
Hargrave, P.J., McEllin, M.: 1975, *Monthly Notices Roy. Astron. Soc.* **173**, 37
Hinder, R., Ryle, M.: 1971, *Monthly Notices Roy. Astron. Soc.* **154**, 229
Jaffe, W.J., Perola, G.C.: 1973, *Astron. Astrophys.* **26**, 423
Laan, H. van der, Perola, G.C.: 1969, *Astron. Astrophys.* **3**, 468
Pacholczyk, A.G.: 1970, Radio Astrophysics, W.H. Freeman and Co.
Perley, R.: 1977, Ph. D. Thesis, University of Maryland
Sandage, A.: 1967, *Astrophys. J.* **150**, L145
Sandage, A.: 1972, *Astrophys. J.* **178**, 25
Schilizzi, R.T., Miley, G.K., van Ardenne, A., Baud, B., Bååth, L., Rönnäng, B.O., Pauliny-Toth, I.I.K.: 1979, *Astron. Astrophys.* **77**, 1
Weiler, K.W., van Someren Gréve, H.W., Piersma, Th.R.: 1973, Netherlands Foundation for Radio Astronomy – ITR 117
Wilkinson, P.N.: 1972, *Monthly Notices Roy. Astron. Soc.* **160**, 305
Willis, A.G., Strom, R.G.: 1978, *Astron. Astrophys.* **62**, 375 (Paper I)
Willis, A.G., Strom, R.G., Wilson, A.S.: 1974, *Nature* **250**, 625
Wyndham, J.D.: 1966, *Astrophys. J.* **144**, 459
Zwicky, F., Herzog, E.: 1966, Catalogue of Galaxies and of Clusters of Galaxies, Vol. III, California Institute of Technology